LA-UR-19-32669
Approved for public release; distribution is unlimited.

Title: Skid Testing FY2019 Report

Author(s): Pederson, Michelle Nicole
Parker, Gary Robert Jr.
Holmes, Matthew David

Intended for: Report

Issued: 2019-12-20

Disclaimer:
Los Alamos National Laboratory, an affirmative action/equal opportunity employer, is operated by Triad National Security, LLC for the National Nuclear Security Administration of U.S. Department of Energy under contract 89233218CNA000001. By approving this article, the publisher recognizes that the U.S. Government retains nonexclusive, royalty-free license to publish or reproduce the published form of this contribution, or to allow others to do so, for U.S. Government purposes. Los Alamos National Laboratory requests that the publisher identify this article as work performed under the auspices of the U.S. Department of Energy. Los Alamos National Laboratory strongly supports academic freedom and a researcher's right to publish; as an institution, however, the Laboratory does not endorse the viewpoint of a publication or guarantee its technical correctness.

Skid Testing FY2019 Report

Pederson, Michelle N.
Parker, Gary R.
Holmes, Matthew D.

Los Alamos National Laboratory

M-6 Explosives Applications and Special Projects
High Explosives Thermal and Mechanical Response Team

November 19, 2019

Abstract

The Skid Test is an experiment that impacts an explosive charge obliquely upon a gritty target in order to deliver a frictional ignition stimulus. At Los Alamos, the Skid Test has been used since 2011 to test myriad explosives, drop heights, impact angles, target materials, target coatings, and other variables. In FY19, forty-four tests were performed. The focus was twofold: 1) investigate the possibility that grit pre-embedded into PBX 9501 can create ignitions when impacting a gritty soft-rubber surface, via grit-grit interactions; 2) test the HMX-based UK explosive EDC37 in typical Skid Test conditions.

Thirty-one tests were performed with grit pre-embedded in PBX 9501, dropped onto gritty soft rubber targets. No ignitions were observed in any of the tests. Previously, nominally identical tests were performed, except lacking the pre-embedded grit, and no ignitions were observed in those tests. Post-mortem analysis suggests that grit-grit collisions are common, yet still fail to produce ignitions. We hypothesize that the softness of the rubber target fails to provide sufficient normal force for frictional heating, regardless the grit-grit collisions.

Eleven tests with EDC37 were conducted in total, at drop heights of 9 in, 6 ft, and 9 ft and with grit diameters of 75-150 μm, 150-250 μm, 250-500 μm, and 500-1000 μm. Ignition of hotspots followed by quench was observed in a single test at an incident angle of 14° and effective drop height of 9 ft. These results demonstrate that EDC37 is safer—i.e. less prone to ignition—than other conventional high explosives tested to date, including PBX 9501.

Table of Contents

1. Introduction **3**
2. Summary of prior Skid Testing at LANL (2011-2018) **3**
2.1. Parameter Space of Prior Testing 4
2.2. Prior Publications 4
3. Purpose of FY19 Testing **4**
3.1. Pre-embedded grit impacting gritty soft rubber surface 4
3.2. Testing EDC37 (a UK HMX-based PBX composition) 6
4. Experiment **6**
4.1. Design 6
4.1.1. Pendulum **6**
4.1.2. Target **7**
4.1.3. Explosive **7**
4.2. Diagnostics 8
4.2.1. High-speed video **8**
4.2.2. Force Transducers **8**
4.2.3. Blast Gauges **8**
4.2.4. Still Photography **8**
5. FY19 Results and Analysis **9**
5.1. Phase I: PBX 9501 with pre-embedded grit impacting gritty, soft-rubber targets 9
5.2. Regarding Hardness 14
5.3. Phase 2: Tests with EDC37 16
6. Conclusions **21**
7. Future Work **21**
8. Acknowledgments **22**
9. Data Requests **22**
10. References **22**
Appendix A: FY 19 Test Record **24**
Appendix B: CAD Illustrations of the Pendulum Apparatus **26**
Appendix C: Images of the Pendulum Apparatus **29**
Appendix D: Rex Gauge Company Durometer **31**

1. Introduction

Dropped explosive charges have been implicated as the cause of multiple deadly historical accidents. The Skid Test was developed in response to two accidents that occurred in the year 1959, one at Los Alamos and one at AWRE in the UK, in which hemispherical charges of HMX-based conventional high explosive killed workers [1-5]. In both accidents, it is believed that the explosives fell from a height of a few feet to impact the ground at a glancing angle. These analyses were based on post-mortem investigation of fragments, as no eye-witnesses lived to describe either incident.

In a *low-velocity* mechanical impact of conventional secondary high explosive, there are two viable ignition mechanisms:

1. Shear/viscous heating internal to the explosive, caused by rapid crushing deformations that induce large velocity gradients within the material. This mechanism typically requires a high impact velocity combined with high confinement, which are difficult to achieve in human-related accident scenarios. It has been determined that this is *not* the ignition mechanism responsible for explosive reaction in the Skid Test results [6,7]. For other insults in which shear heating plays a role, consult references [8] and [9].

2. Frictional heating of two high-melting point materials that are in contact with the explosive. This mechanism can localize heating at very low impact velocities, and was first explored in a seminal paper by Dyer and Taylor [10]. This ignition mechanism can be accessed with numerous plausible accident scenarios, e.g. drops, trips, falls, etc., and is the ignition mechanism explored in Skid Testing.

2. Summary of prior Skid Testing at LANL (2011-2018)

The original Skid Test design consists of a pole and cable "swing set" [11,12]. The charge is remotely dropped and swings into a sheet of plate glass, thereby impacting at an oblique angle which causes the charge to slide on the surface of the glass.

The modern version of the Skid Test experiment at Los Alamos was designed and built in 2010 to improve upon the historical apparatus employed at Pantex Plant and elsewhere. The original impetus for building a LANL Skid Test was to answer outstanding questions regarding confusing results and misconceptions[1] of the ignition mechanisms that dominated the explosive response with an apparatus that could deliver a more controlled impact with additional diagnostics.

In the first year of its use, 2011, the LANL version of the pendulum conclusively demonstrated that no ignitions are observed on clean glass impacts with clean pieces of PBX 9501 (i.e. in the absence of any grit contaminants) [14], thereby reinforcing the historical findings of Dyer and Taylor. In the years following, it has been used to test impacts on various substrates, angles, drop-heights, explosives, contaminants, charge geometries, and surface preparations. Over five-hundred test have been performed to-date.

[1] For an example of the misconceptions and mistaken analyses, consider references [12,13], in which the role of grit as the heat localization mechanism is unacknowledged.

2.1. Parameter Space of Prior Testing

The following list summarizes the range of test parameters that have been explored since the pendulum was placed into service in 2011 (test variables from this report are included).

1. Explosive Compositions
   a. PBX 9501
   b. Aged PBX 9501
   c. PBX 9502
   d. PBX 9407
   e. LX-10
   f. LX-14
   g. PBX 9404
   h. EDC37
2. Drop height
   a. 9 in.
   b. 12 in.
   c. 18 in.
   d. 36 in.
   e. 6 ft.
   f. 9 ft.
   g. 12 ft
3. Target material
   a. glass
   b. Sapphire
   c. 6061 Aluminum
   d. Anodized 6061 aluminum
   e. Electro-less nickel-plated 6061 aluminum
   f. Mild steel
   g. Polycarbonate
   h. Delrin
   i. Adiprene rubber (harnesses ranging from D12 to D70)
   j. Various flooring materials, including tile, vinyl, norament, rubber, and polymers.
4. Grit sizes:
   a. 500-1000 μm ("cut 1")
   b. 250-500 μm ("cut 2")
   c. 100-250 μm ("cut 3")
   d. 75-100 μm ("cut 4")
5. Exotic grit arrangements
   a. Single grit particle
   b. Two side-by-side grit particles
   c. Four grit particles, arranged in a square
   d. Monolayer clusters of particles

2.2. Prior Publications

The following publications document prior work conducted on the LANL Skid Test apparatus.

[14] FY13 Report: "The Effect of Grit on Frictional Heating During Oblique Impacts with PBX 9501"

[15] FY14 Report: "The Effect of Grit on Frictional Heating During Oblique Impacts with PBX 9501 Fiscal Year 2014 Update"

[6] 15th International Detonation Symposium: "Friction-induced heating and ignition of PBX 9501"

[16] Journal article in Reliability Engineering and System Safety: "Grit-mediated frictional ignition of a polymer-bonded explosive during oblique impacts: Probability calculations for safety engineering"

[17] FY15 Report: "Oblique Impacts with PBX 9501: Fiscal Year 2015 Skid Testing Results"

[18] FY16 Report: "Oblique Impacts with PBX 9404, LX-14, LX-10 and Aged PBX 9501"

[19] FY18 Report: "Oblique Impacts with PBX 9501, PBX 9407, Comp B and Naturally Aged PBX 9501 Hemi Shells"

[20] 16th International Detonation Symposium: "Magnitude of Response to Frictional Ignition by Oblique Impact of High Explosives Formulations"

3. Purpose of FY19 Testing

3.1. Pre-embedded grit impacting gritty soft rubber surface

Previous experimentation indicated that sufficiently soft rubber targets successfully mitigate explosive reaction, even when those targets are contaminated with grit [15]. These previous results are summarized in Figure 1. In tests using rubber targets that are softer than the explosive, it has been observed that the grit present on the rubber surface is preferentially embedded in the rubber surface, but not into the PBX 9501 during the dynamic impact. When all of the grit is embedded in the rubber target surface, and none is embedded in the HE, there is no opportunity during the impact for grit-grit collision, which has been

implicated as the ignition mechanism on polymer target impact surfaces. Therefore, it has been hypothesized that the lack of reaction results from the lack of grit-grit collisions in these PBX 9501 impacts on soft rubber. Consequently, rubber of hardness lower than that of PBX 9501 has been recommended as a possible mitigation for explosive reaction during skid insults.

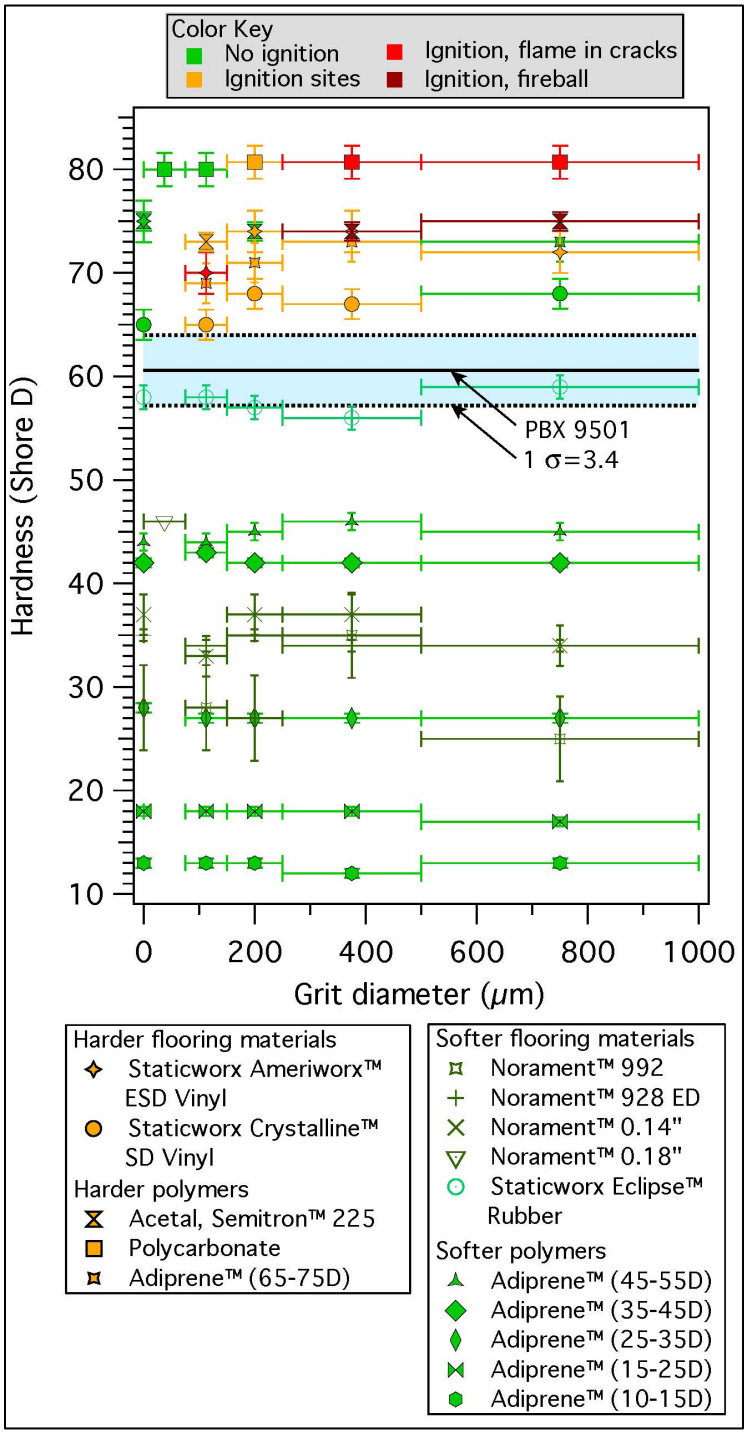

Figure 1. Results from previous Skid Testing with various Polymer targets.

However, a question remained: consider a scenario in which grit is already embedded in the surface of the explosive, and then dropped against a gritty soft rubber surface? Will the pre-embedded grit in the explosive permit the grit-grit collisions that tests where the soft rubber targets were the sole contaminate surface lacked observation of? Testing in FY19 was conducted to address this scenario.

3.2. Testing EDC37 (a UK HMX-based PBX composition)

The effect of binder on the sensitivity to ignition and post-ignition violence is an important subject of ongoing explosive safety research. Previously, it has been demonstrated that LX-10, LX-14, and PBX 9404 all react more violently than PBX 9501 in the Skid Test [20,18]. Since the HMX fill-fraction of these explosives is nearly identical (95%), the difference in explosive response is attributed to the differing binders, with a focus on the mechanical properties conveyed to the explosive composition by those binders.

The UK explosive EDC37 is an attractive candidate for binder research and its effect of post-ignition response, as it is quite different from the Viton and Estane binders used in the US compositions. Additionally, EDC37 is rumored to be safer than PBX 9501 to low-velocity mechanical insult; Skid Testing of EDC37 was required to confirm this claim, and if true, help elucidate the properties that dominate the explosive response.

4. Experiment

4.1. Design

4.1.1. Pendulum

The pendulum apparatus has undergone many changes and improvements since it was first put into service in 2011. The design has been described in detail previously [15]. Here, select details of the current state of the pendulum are re-documented.

For images and illustrations to accompany this discussion please consult Appendix B and Appendix C. The pendulum has a 15 ft long rigid arm, permitting a maximum effective drop height of 12 ft. An electric winch is used to hoist the arm. The hoisting cable extends from the winch—which is bolted to the base—to the upper axle of the pendulum arm, where it is wrapped around a 16 in diameter disc. The cable is fastened to the winch line with a mechanical latch. The latch is fitted with a pneumatic actuator which allows it to be released remotely.

An inclinometer is used to sense the angle of the pendulum arm. A microprocessor control circuit is used to convert the angle into an equivalent drop height, which is displayed on an LCD screen while operating the winch. This is an impact velocity match: "equivalent height" of 6 ft means that the impact velocity of the drop matches that which would occur if an object were vertically dropped 6 ft in free-fall. Impact velocity for a vertically dropped object in free-fall, ignoring air resistance, is given by $v = \sqrt{2ad}$, where v is impact velocity, a is gravitational acceleration, and d is the drop height. Figure 2 shows a plot of this expression for impact velocity in the drop-height regime of interest for Skid Test experiments.

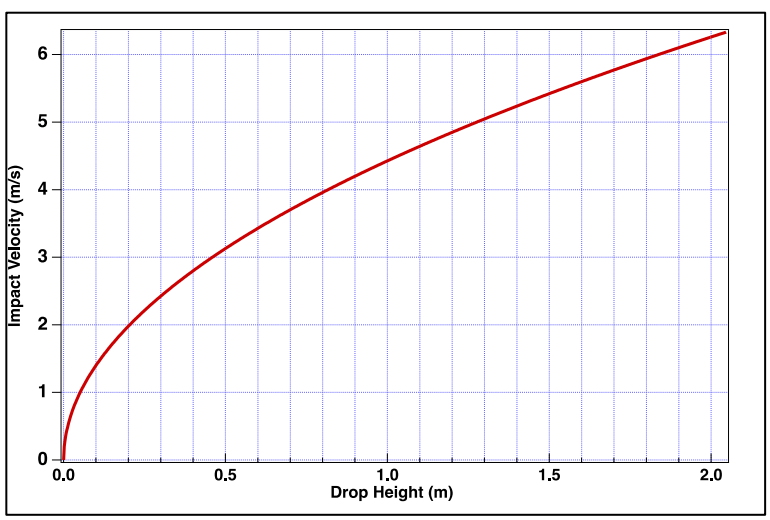

Figure 2. Basic kinematics: impact velocity for a given free-fall drop height (in the absence of air resistance).

The assembly containing the explosive must be secured to the end of the pendulum arms during the first portion of the drop, or it will fall off the pendulum arms onto the ground when dropped. Solenoids are used to pin the vehicle assembly to the arm ends. These solenoids are retracted as the arms are dropping, immediately before impact. This allows the vehicle assembly to impact and bounce off the target with natural kinematic motion, rather than being "driven" into the target with the entire momentum of the pendulum arms. A custom "solenoid retraction box" is used to source the current for rapid retraction of the powerful solenoids. This solenoid retraction box is located in a protective enclosure next to the pendulum (each solenoid is ~ 1 ohm and is excited with ~50 V, for a brief current of ~50 A) and is remotely actuated with a low-voltage trigger signal.

The pendulum arm is dropped by pressurizing the pneumatic actuator on the release latch. A simple continuity circuit is wired between the latch and the latched shackle (which is dropped when the latch opens). This circuit informs the control system that the arm has been dropped and is in free-fall. The control system implements a five-term expansion of the solution to the pendulum equation in order to determine the time interval between drop and impact. This time interval is calculated continuously as the pendulum arms are hoisted. Before the arm is dropped with the pneumatic release, the control system is placed into an "armed" status (with a key switch). Approximately 100 ms before the calculated impact time, the control circuit sends a trigger signal to the solenoid retraction system.

Photodiode transmitter/receiver sensor pairs are mounted on the solenoid housings on each side, and provide an independent signal to confirm that solenoids have been retracted (these signals are used for monitoring purposes, and play no role in the control circuit). This provides confirmation that no additional energy from the pendulum arm motion is added to the impact.

4.1.2. Target

The most common target is a transparent 6 in. diameter by 1.5 in. total thickness piece of glass (comprised of two laminated layers of 0.75 in. thick tempered plate glass). This glass rests in a counter bore in a stainless steel impact frame. The angle of this impact frame can be adjusted; details of this arrangement are visible in Figure 34 and Figure 35.

The sand used for this testing is a high-quality, commercially available silica sand product (Grade: Federal Fine, U.S. Silica Company, PO Box 577, Ottawa, IL). This is the same sand that is used for Skid Testing at the Pantex Plant, mined from the St. Peter Sandstone formation near Ottawa, IL. It is over 99% pure quartz, with well-rounded, edges making it relatively strong under compressive loading. To control grit diameter, the sand was sorted into the following size fractions using ASTM E11 U.S. Standard Test Sieves (Precision EForming, LLC, Cortland, NY 13045): 1000-500 μm, 500-250, μm, 250-150 μm, 150-75 μm and <75 μm. Micrographs of each sieve-cut are shown in reference [15].

When sanded, the target is prepared by misting with a sugar water solution (50/50 by volume) then wiping dry, leaving a slightly tacky surface to which the sand can adhere. Sand of a chosen sieve cut is then sprinkled by hand across the surface to attain a visually uniform areal density. An effort is made to reach an areal density similar to that of testing performed since 2011, but there is no specification for the target coverage density.

4.1.3. Explosive

The most commonly tested sample geometry is the "cupcake" (Figure 3). The cupcake is uniaxially pressed using a custom die set. The canonical PBX 9501 cupcake has a nominal density of 1.83 g/cc and mass 249 g.

The explosive sample is held in a Delrin "vehicle." An aluminum tube passes through the center of the vehicle. Delrin mounting blocks are fastened to the end of the aluminum tube. The mounting blocks mate to shelves on the arm attachments. These components are illustrated in Figure 36-Figure 38. The overall mass of the vehicle assembly, not including the explosive sample is 13.5 lbs (6.1 kg).

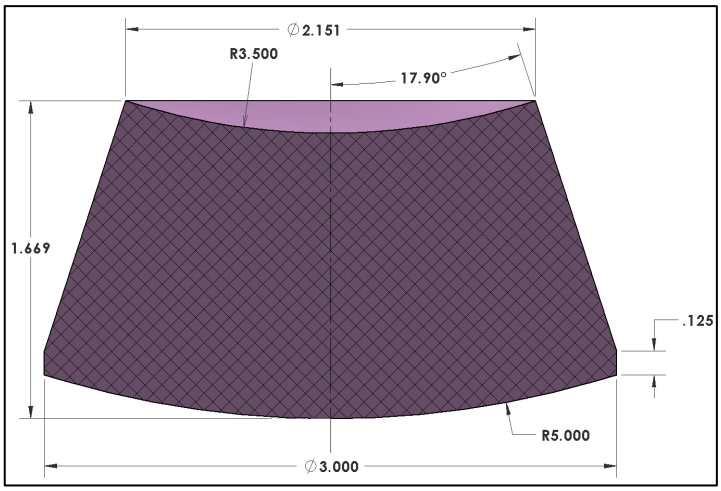

Figure 3. Explosive geometry; the "cupcake," with dimensions.

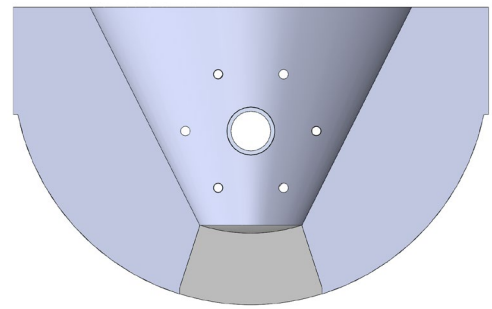

Figure 4. Cross section of cupcake mounted in vehicle.

4.2. Diagnostics

4.2.1. High-speed video

The primary diagnostic is a high-speed video camera view through the transparent glass target. Typically, a Vision Research® Phantom™, model V2512 is used with a zoom lens at 560 mm focal length at an aperture of f22 to obtain frame rates of 110,000 fps at a resolution of 384 px by 384 px. A custom-built LED light ring is mounted below the glass target to provide the considerable illumination required for a well-exposed image at this frame rate. The LED lighting is turned on just before the drop, and off immediately afterwards, in order to avoid overheating the LED elements (the custom ring is designed only for intermittent rather than continuous duty use).

A second high-speed video camera is used to record a wide side-view of the impact, providing a record of fireballs and ejecta.

4.2.2. Force Transducers

The glass target rests in a stainless-steel cradle. This cradle rests atop four force transducers (PCB® piezotronics™ model 208C05, range 22.24kN) that measure the force normal to the target axis. The cradle is abutted to a fifth, lateral force transducer (PCB® piezotronics™ model 208C05, range 22.24kN) to measure the translational force. The arrangement of these components is depicted in Figure 35 and Figure 36.

4.2.3. Blast Gauges

Diagonally above and preceding the impact point, stagnation plate blast gauges are mounted, facing the impact location, in an effort to quantify the violence of the reaction. The location of the stagnation plate relative to the experiment can be seen in Figure 39. These gauges have proven useful to rank relative violence of reactions, though the data from these gauges must be interpreted carefully, as the fireballs that sometimes result are not spherically symmetric (this is unavoidable owing to the experiment geometry).

4.2.4. Still Photography

Still photographs are taken of gritty targets before and after testing. These photographs can be used to determine, via image-analysis, statistics regarding the sand diameter, areal density, and areal distribution. Still photographs also reveal gouge tracks in glass targets and the locations of embedded sand grains.

5. FY19 Results and Analysis

All tests reported here were executed August 2019 in Los Alamos, NM where the average humidity for the month was 10% and the daily average high temperature was 78 ºF (26 ˚C).

5.1. Phase I: PBX 9501 with pre-embedded grit impacting gritty, soft-rubber targets

Adiprene® polymer sheet was chosen as the soft-rubber target material. Adiprene is a cured liquid urethane with desirable properties for Skid Testing: a) it is transparent b) it can be easily formulated at varying hardness in the desired range. Two hardnesses of Adiprene were used for the testing reported here: Shore 44D and Shore 25D[2]. A 0.25 in. thick disc of Adiprene was bonded to a 1 in. thick glass disc using a clear RTV Silicone adhesive. This Adiprene is the polymer used at Pantex for tooling and impact mitigation on surfaces.

These same Adiprene targets have been tested in previous Skid Tests with grit only on the impact surface and resulted in no ignitions [15]. Figure 1 recaps these results. Post-mortem examination of the explosive and soft Adiprene targets in these previous tests indicated that all of the grit was preferentially embedded into the rubber, and none of the grit embedded in the explosive surface, thereby preventing the grit-grit collision heating mechanism that is responsible for ignition on harder polymer target surfaces. The dynamics of this impact scenario are illustrated in Figure 5.

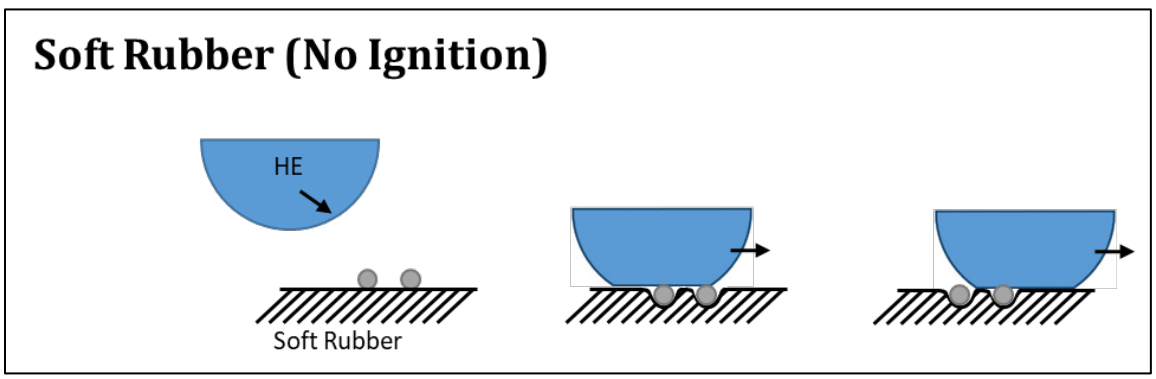

Figure 5. Dynamics of an explosive impacting a *soft* rubber surface covered with grit particles.

Note that ignitions have been observed on gritty rubber surfaces *when the rubber surface was sufficiently hard*. This scenario is illustrated in Figure 6 and was thoroughly addressed in [15]. However, in this report we concern ourselves with the potential for ignition on *soft* rubber surfaces.

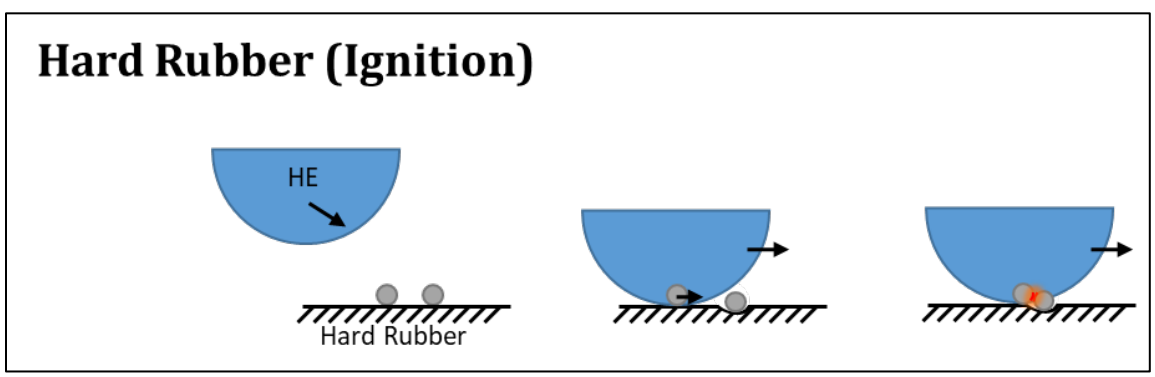

Figure 6. Dynamics of an explosive impacting a *hard* rubber surface covered with grit particles.

[2] At Pantex plant the Adiprene is cured with dye to visually differentiate hardness. The 44D is dyed black and the 25D is dyed gray. Pantex plant prepared these Adiprene samples for us without the dyes in order to maintain optical clarity.

To encourage grit-grit collisions on soft rubber impacts, grit was pre-embedded into the explosive surface. The resulting impact scenario is illustrated in Figure 7.

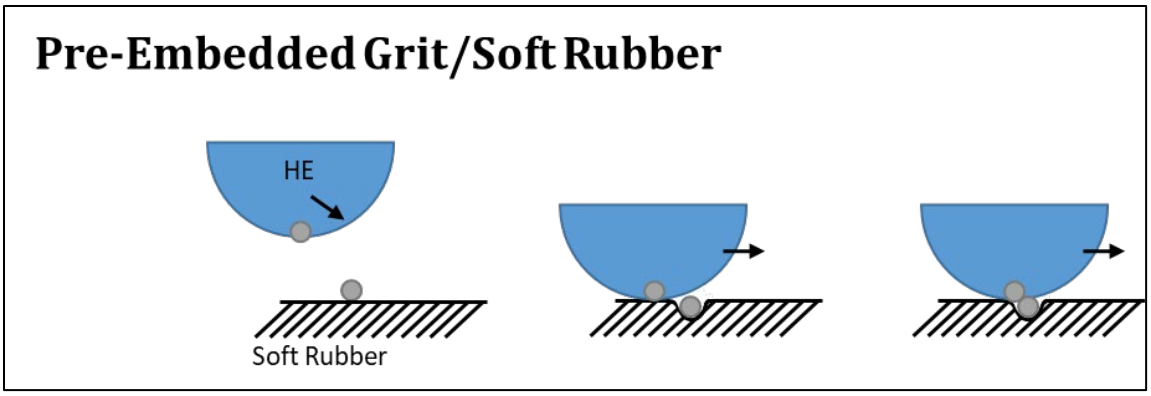

Figure 7. Dynamics of pre-embedded grit in explosive impacting a soft rubber surface covered with grit particles.

Cut 2 sieved sand (250-500 μm diameter) was embedded into the surface of the PBX 9501 by hand using a delicate procedure. A 0.75 inch diameter circle was drawn on the center of the HE with a permanent marker. A single particle of grit was then placed inside the circle with tweezers. A 0.25 inch diameter Delrin® rod was used to gently press the grit into the HE. This process was repeated until an estimated 40 grit particles were embedded inside the circle with a uniform areal density (Figure 9).

A total of thirty-one pre-embedded grit tests were performed. The results can be found in Table 1 and are visually organized in Figure 14 and Figure 15. No ignition was observed in any of the drops. The drops were performed with three impact surface hardnesses, four grit sizes on the impact surface, and two incident angles. Constants include the explosive type (PBX 9501), drop height (6 ft), and size of grit embedded into the HE (250-500μm).

Seventeen drop tests were performed at an incident angle of 45° and fourteen drop tests were performed at an incident angle of 14°. Most of these tests were performed using the harder of the two Adiprene impact surfaces (black D44). The largest grit cuts—250-500 and 500-1000 μm—were repeated 6 times per cut at each incident angle. Tests with the lower hardness impact surface were repeated only twice per grit cut (250-500 and 500-1000 μm). The rest of the grit cuts (75-100 and 100-250 μm) were tested once at each incident angle.

Although no ignitions were observed, post-mortem visual inspection of the explosive and rubber surfaces reveals that grit-grit collisions are occurring during the impact. This is evident in the photographs, particularly Figure 11, where it is clear that clumps of grit have formed on the explosive surface. Figure 13 photographs a rubber surface after testing, showing that grit remains.

Table 1. Test details and results for PBX 9501 grit on grit Skid Test study. The second column includes the nominal hardness; the third column shows the hardness measured at the firing site when the test was performed.

Drop #	Adiprene Impact Surface	Durometer Hardness (Shore D)	Nominal Drop Height (ft)	Incident Angle (deg.)	Grit Size on Impact Surface (μm)	Grit Size on HE Surface (μm)	Result
542	Black 44D	41	6	45	500-1000	250-500	No Ignition
543	Orange 45D	46	6	45	500-1000	250-500	No Ignition
544	Black 44D	40	6	45	500-1000	250-500	No Ignition
545	Black 44D	40	6	45	500-1000	250-500	No Ignition
546	Black 44D	44	6	45	500-1000	250-500	No Ignition
547	Black 44D	40	6	45	500-1000	250-500	No Ignition
548	Black 44D	40	6	45	250-500	250-500	No Ignition
549	Black 44D	43	6	45	150-250	250-500	No Ignition
550	Black 44D	43	6	45	75-150	250-500	No Ignition
551	Gray 25D	27	6	45	500-1000	250-500	No Ignition
552	Gray 25D	27	6	45	500-1000	250-500	No Ignition
553	Black 44D	41	6	45	250-500	250-500	No Ignition
554	Black 44D	40	6	45	250-500	250-500	No Ignition
555	Black 44D	39	6	45	250-500	250-500	No Ignition
556	Black 44D	39	6	45	250-500	250-500	No Ignition
557	Black 44D	39	6	45	250-500	250-500	No Ignition
558	Black 44D	39	6	45	250-500	250-500	No Ignition
565	Black 44D	NM	6	14	500-1000	250-500	No Ignition
566	Black 44D	39	6	14	500-1000	250-500	No Ignition
567	Black 44D	41	6	14	500-1000	250-500	No Ignition
568	Black 44D	39	6	14	500-1000	250-500	No Ignition
569	Black 44D	39	6	14	500-1000	250-500	No Ignition
570	Black 44D	39	6	14	500-1000	250-500	No Ignition
571	Gray 25D	39	6	14	250-500	250-500	No Ignition
572	Gray 25D	39	6	14	250-500	250-500	No Ignition
573	Black 44D	39	6	14	250-500	250-500	No Ignition
574	Black 44D	39	6	14	250-500	250-500	No Ignition
575	Black 44D	39	6	14	250-500	250-500	No Ignition
576	Black 44D	39	6	14	250-500	250-500	No Ignition
577	Black 44D	39	6	14	150-250	250-500	No Ignition
578	Black 44D	39	6	14	75-150	250-500	No Ignition

Table 2. Images of PBX 9501 grit-grit Skid Test with ¾ inch circle.

Figure 8. Pre-embedded grit in PBX 9501 (Drop 543).

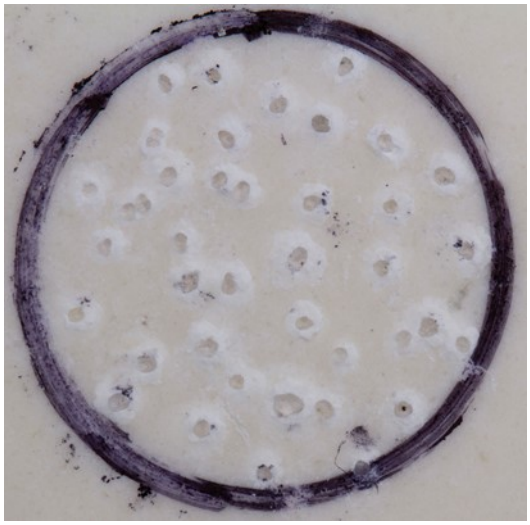

Figure 9. Close up of pre-embedded Cut 2 grit in PBX 9501 (Drop 543).

Figure 10. Grit in PBX 9501 post drop (Drop 542).

Figure 11. Close up of grit in PBX 9501 post drop (Drop 544).

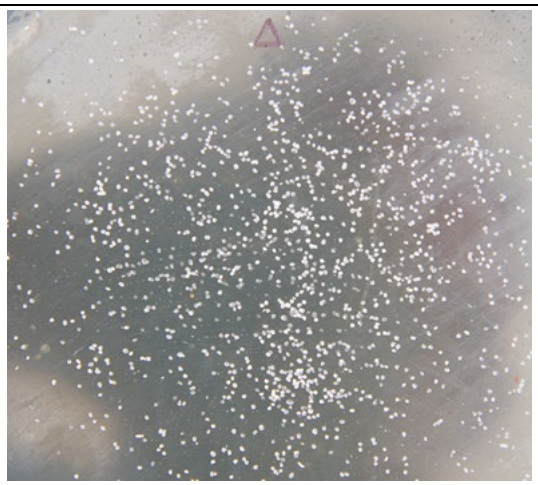

Figure 12. Cut 2 grit on rubber pre drop (Drop 544).

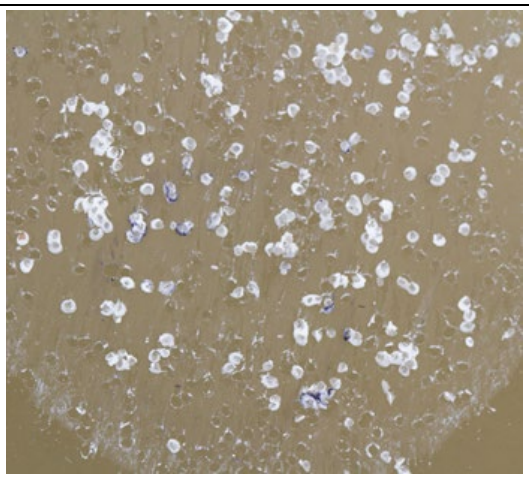

Figure 13. Close up of Cut 2 grit on rubber post drop (Drop 544).

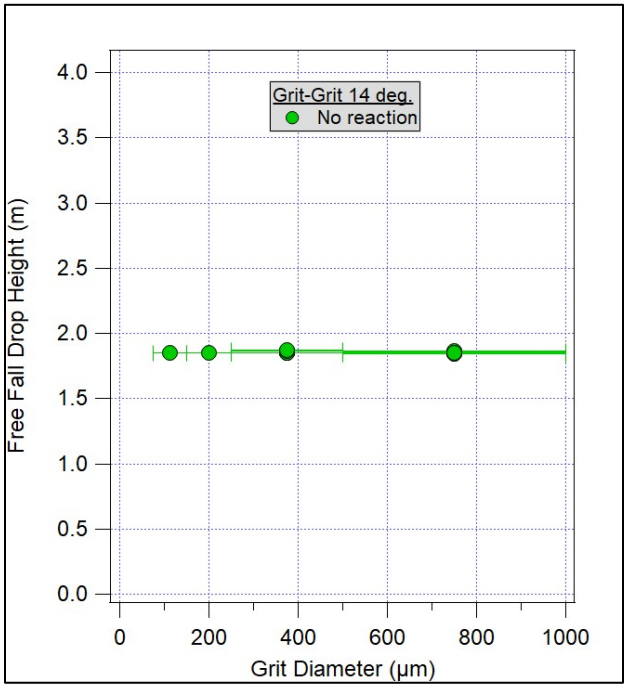

Figure 14. Test results of HE with pre-embedded grit impacting gritty soft rubber at a 14° incident angle.

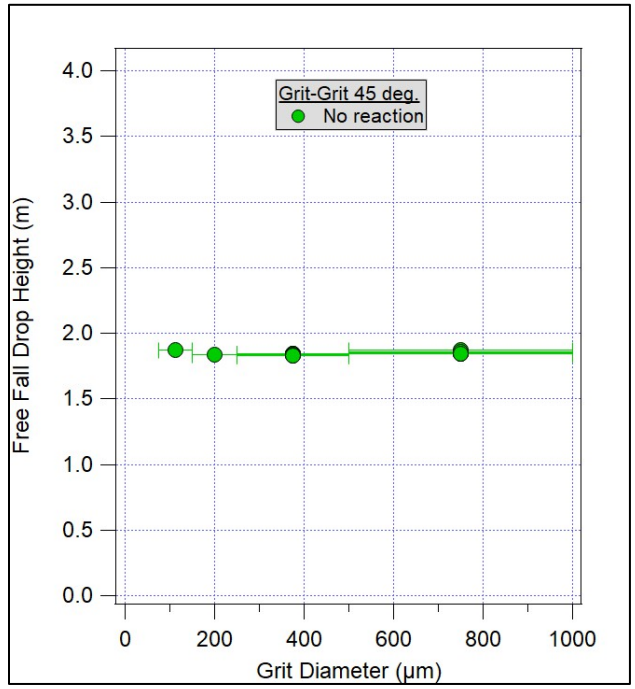

Figure 15. Test results of HE with pre-embedded grit impacting gritty soft rubber at a 45° incident angle.

Evidently, grit collisions are not producing ignitions in these soft-rubber impacts. We therefore hypothesize that the reason why soft rubber mitigates ignition is not only because it eliminates grit-grit collisions, but also because insufficient normal force is exerted on the grit particles to cause sufficient frictional heating when collisions do occur. This hypothesis is illustrated in Figure 16, where it is contrasted with the scenario of impacts on harder rubber in which grit-grit collisions have been observed to cause ignition [15].

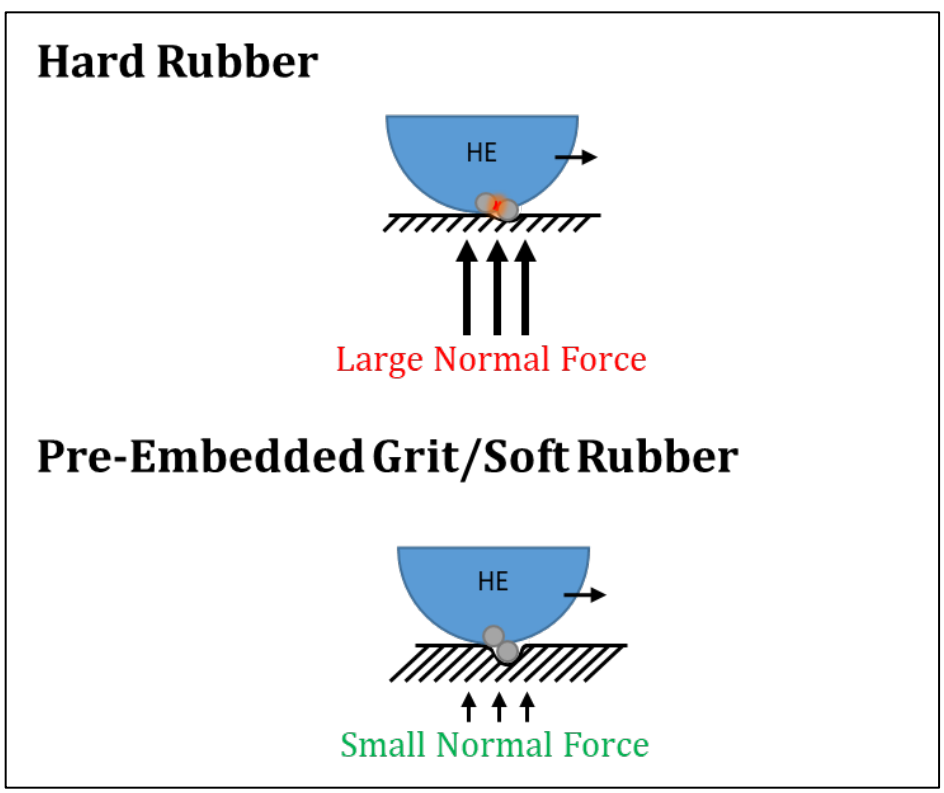

Figure 16. Illustration of the hypothesis that normal force influences ignition of HE impacting rubber surfaces.

Drop 570 yielded an interesting observation. Figure 17 shows a sequence of stills from the high-speed video record. A "sparkle" was observed in a single frame of video during this drop. This "sparkle" was dimmer than a typical ignition hot spot, and white, rather than the typical yellow tint of a hotspot, so the cause is likely due to specular reflection off a rotating grit face. This sparkle could also be caused by triboluminescence, due to crushing of a grit particle, but we deem this less likely owing to the reduced normal force achievable on the rubber substrate. This phenomenon has been observed with inert "no HE involved" tests in previous years [14]. Although ignition in this test cannot be completely ruled out, the evidence indicates that this "sparkle" was not an ignition, and it is recorded as a "no ignition" in the test results table.

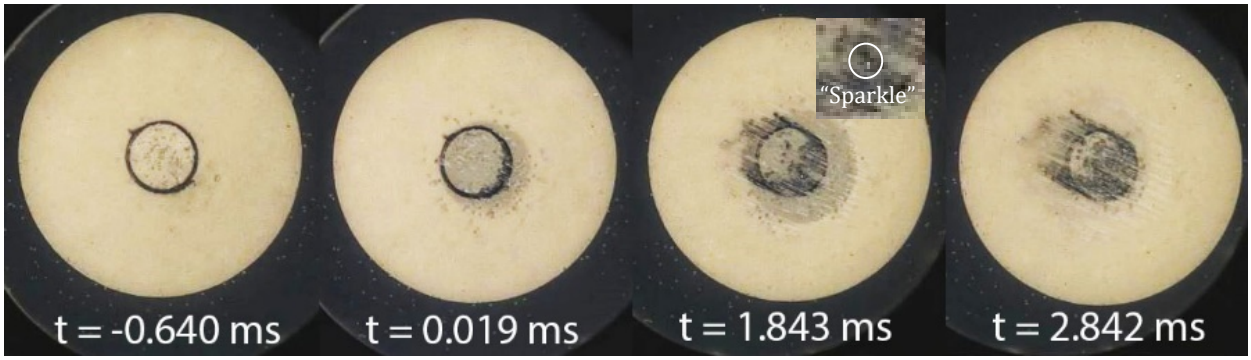

Figure 17. Frame sequence from a high-speed video record, viewing through the rubber (Drop 570). Circles in the image were drawn on the explosive with permanent marker; diameter of the circle is 0.75 in.

5.2. Regarding Hardness

Polymer "hardness" is not an absolute material property, rather it is only defined with respect to a particular type of testing tool. The Shore D indentation hardness scale is appropriate for polymer bonded explosives, and we have used exclusively this scale for our measurements and hardness comparisons.

The Shore D test tool is a conical indenter, with shaft diameter 1.1 – 1.4 mm, a 30° cone angle, and a tip radius of 0.1 mm. A spring force of 44.45 N pushes the indenter into the material and the force as a function of deformation is measured, from 0 to a maximum distance of 2.54 mm [21] (indentation of 0 mm results in a Shore D hardness of 100, indentation of 2.54 mm results in a Shore D hardness of 0, scaling linearly). The tool geometry is shown in Figure 18.

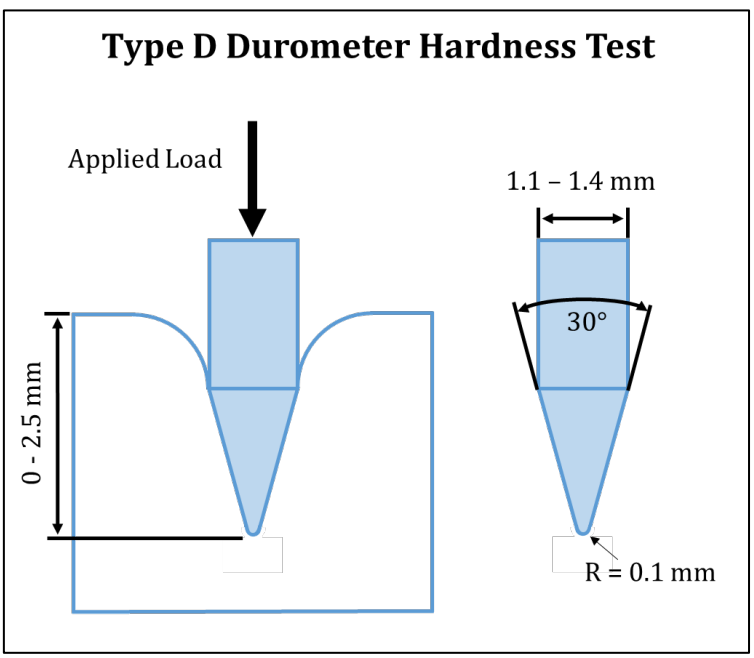

Figure 18. Type D durometer geometry.

During FY14 testing, we reported a nominal hardness for PBX 9501 of 69±1.4 Shore D[15], using a single calibrated analog handheld device for those measurements. The device used was Model 2000 Max-Hand™ Durometer Type D manufactured by Rex Gauge Company®, with NIST-traceable calibration (Appendix D).

However, PBX 9501 hardness measurements made since FY14 have been consistently lower than the originally reported value. A brief investigation was conducted to quantify the variation of hardness within an individual explosive sample and between explosive samples. The hardness of a single PBX 9501 sample was measured in 20 separate locations using the same tool as used in FY14. These measurements were taken on room temperature samples (20˚C ± 2˚C). The hardness of the single sample was found to have a mean of 60.8 Shore D with a standard deviation of 2.6. A second PBX 9501 sample was measured in 20 separate locations to have a mean of 63.5 with a standard deviation of 3.0. This process was repeated for two separate samples of EDC37. A summary of the hardness measurements is shown in Table 3. These hardness values are consistent with measurements we have made since FY14, so we believe that the original reported hardness of 69 Shore D was erroneous.

Table 3. Explosive hardness measurements.

Composition Sample	Hardness (Shore D)	# measurements	Composition Average
PBX 9501 Sample A	60.8 std. dev. 2.6	20	PBX 9501 62 std. dev 2
PBX 9501 Sample B	63.5 std. dev. 3.0	20	
EDC37 Sample A	55.0 std. dev. 2.5	20	EDC37 54 std. dev 2
EDC37 Sample B	52.3 std. dev. 4.5	20	

The standard deviations reported in the above hardness measurements accurately captures the variation of explosive hardness under the conditions that Skid Testing experiments were performed during this FY. There are numerous factors that contribute to the observed variation in hardness:

1) The size of HMX grains in PBX 9501 has a bimodal distribution, with modes of 5 μm and 234 μm [22,23], and the indenter tip has a radius of 100 μm. Therefore, the explosive composition is somewhat inhomogeneous on the scale of the indenter tip.

2) HMX crystals are considerably harder than the binder [24,25], consequently it is to be expected that the hardness measurement will differ depending on whether the indenter tip lands squarely on an HMX crystal versus a binder gap between grains. This has implications for frictional grit heating as well: the grit frictional heating behavior is expected to differ depending on where the grit embeds in the explosive.

3) Hardness changes with the temperature of the material (this is particularly true for polymers). Explosive temperature is not a control variable in Skid Testing; the experiment is conducted outdoors and the samples are generally at, or close to, the ambient outdoor temperature. Skid Testing has been performed in all seasons, and ambient temperatures at the firing site where the experiment is located can vary by ~40 ˚C from winter to summer.

4) The most consistent hardness results are achieved with a table-top system that can repeatedly apply the indenter normal to the sample surface with a precise loading force. In contrast, the results obtained with the handheld tool will vary depending on the angle of incidence with the sample surface, the rate of application, and the peak pressure applied. Different users may obtain systematically varying results from the same tool.

5) The surface of the HE "cupcake" geometry, from which all of our hardness measurements originate, is not flat, and thus not ideal for hardness measurements.

6) Typically a uniaxially pressed part will exhibit a slight radially dependent density variation—parts are denser at the center than at the circumference [26]. The hardness measurement is performed near the edge of the sample, in order to avoid damaging the impact area. If the measurement is too close to the edge, it is conceivable that edge-effects from the uniaxial pressing would be observed. The necessary distance away from the edge to avoid edge effects is unknown.

For the reasons stated above, it is important to be aware of the limitations of hardness testing. Reported hardness numbers are best interpreted only in comparison to other measurements made during the same test period, using the same indenter tool, and ideally employed by the same worker.

5.3. Phase 2: Tests with EDC37

The HMX-based UK explosive, EDC37, had not yet been tested with the LANL Skid Test apparatus. We employed a scoping test matrix to address the primary independent variables, including drop heights, incident impact angle, and grit size.

In total, eleven EDC37 Skid Tests were performed in FY19. Test details and results can be found in Table 4. All tests were performed with a glass impact surface. Several tests were performed at the lowest drop height of 9 in, without reaction. The drop height was raised to 6 ft, and later 9 ft. The majority of the drops were performed at a 45° incident angle (in previous testing with PBX 9501, this angle was shown to cause more explosive response than shallower impact angles). For the final three tests, the incident angle was lowered to 14° to obtain a greater degree of translational motion across the impact surface.

Out of the eleven tests, ignition was observed in only one test: Drop 563. This test occurred at the highest drop height (9 ft), shallower angle (14°), and largest grit size (Cut 1: 500-1000 μm). Figure 19 shows a time-lapse of this drop with respect to trigger time. 390 μs ± 19 μs μs after impact, approximately four hotspots were observed and lasted for a duration of 554 μs ± 19 μs.

These EDC37 results are compared with PBX 9501 in Table 5, from which it is evident that EDC37 is considerably less sensitive to skid insults than PBX 9501.

Table 4. Test details and results for EDC 37 Skid Test study.

Drop #	Impact Surface	Drop Height (ft)	Incident Angle (deg.)	Grit Size (μm)	Result
535	Glass	9 in	45	250-500	No Ignition
536	Glass	9 in	45	250-500	No Ignition
537	Glass	6	45	250-500	No Ignition
538	Glass	6	45	250-500	No Ignition
539	Glass	6	45	500-1000	No Ignition
540	Glass	6	45	150-250	No Ignition
541	Glass	6	45	75-150	No Ignition
560	Glass	9	45	250-500	No Ignition
561	Glass	6	14	250-500	No Ignition
562	Glass	9	14	250-500	No Ignition
563	Glass	9	14	500-1000	Ignition, quench

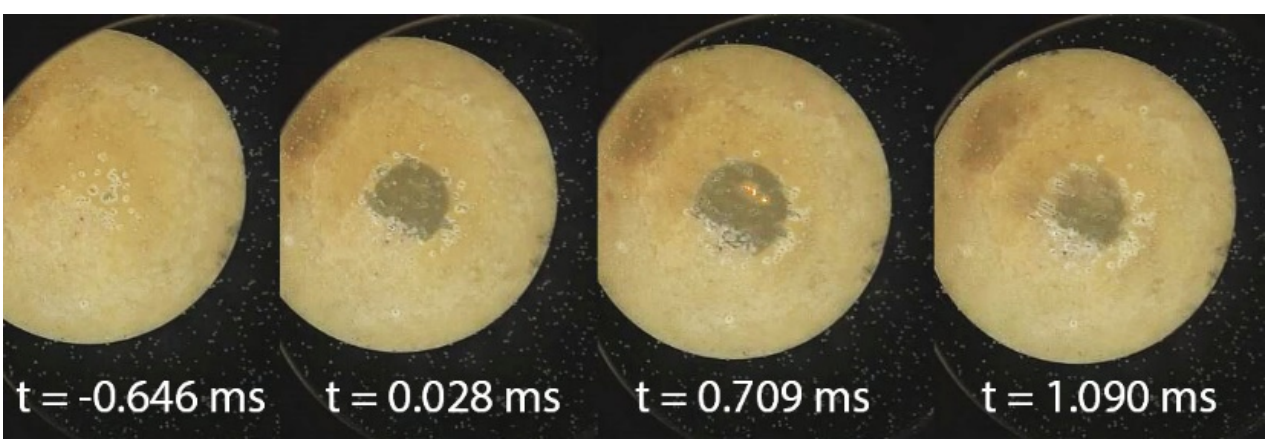

Figure 19. Frame sequence from a high-speed video record, viewing through the glass. This is a low violence response from EDC 37 showing ignition sites, but no propagation in Drop 563.

Table 5. Sensitivity plot comparisons for EDC37 and PBX 9501 Skid Tests.

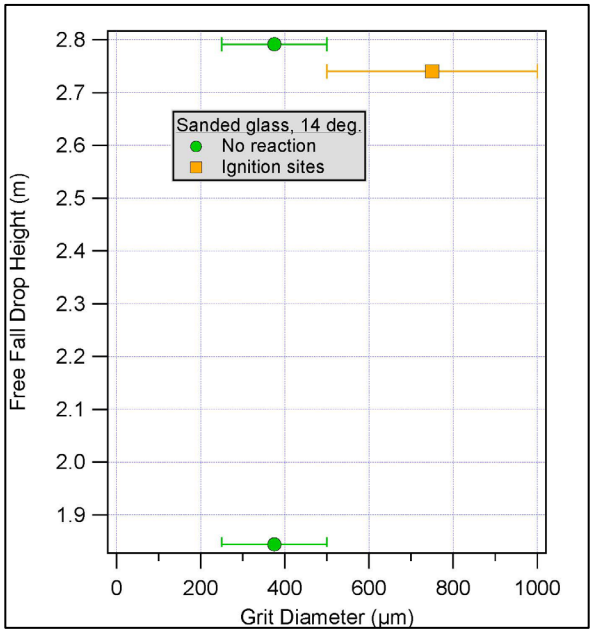

Figure 20. Results for *EDC37* Skid Tests at 14° incident angle.

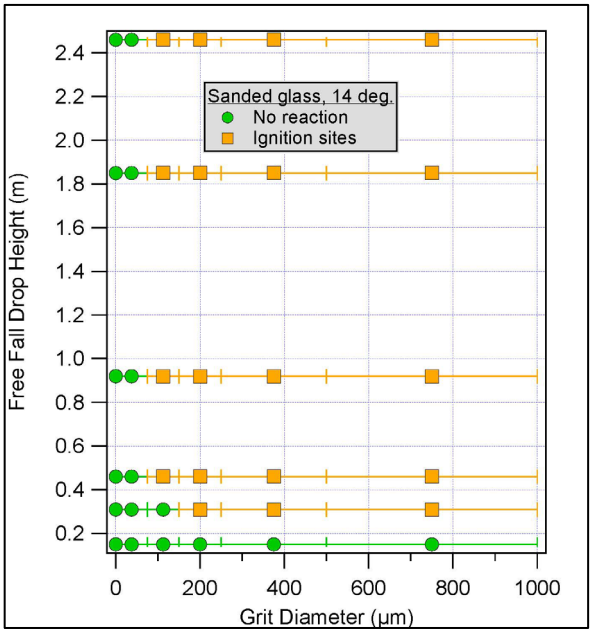

Figure 21. Results for *PBX 9501* Skid Tests at 14° incident angle. These results are from testing performed in 2013-2014.

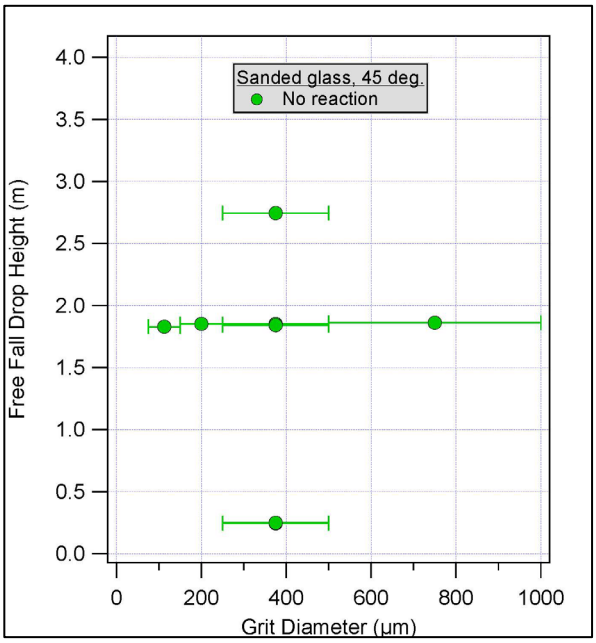

Figure 22. Results for *EDC37* Skid Tests at 45° incident angle.

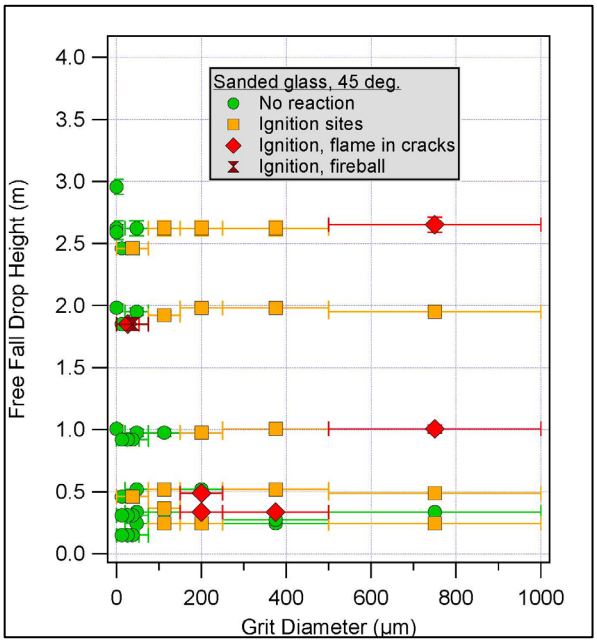

Figure 23. Results for *PBX 9501* Skid Tests at 45° incident angle. These results are from testing performed in 2013-2014.

A single test (Drop 564) with PBX 9501 was performed in this test series, with nominally identical conditions, to rule-out some unknown variation with the FY19 test setup. This test resulted in quenched ignitions, which is consistent with previous results (Figure 21).

Five force transducers are used in Skid Testing to record the force that the HE exerts on the impact surface. Four force transduces are located under each corner of the impact surface mount to record normal force. The fifth force transducer is located at the lateral face of the impact surface mount to record lateral force. This force transducer is more relevant in tests that have an incident angle of 14°, rather than 45°, because the velocity vector ratio (0.25) favors the lateral component of velocity in skid tests that have acute impact angles [17].

Interpreting these force data is challenging: at the ~2 ms timescale of the impact, the frame which supports the target does not behave as an ideally rigid solid. Hence the dynamic structural mechanics of the frame affects the force traces. Often, the four normally-oriented force transducers will not exhibit simultaneous behavior, suggesting that compressive and tensile waves travelling through the supporting frame are not axisymmetric around the center of the glass target.

The average pressure of the impact spot between the HE and the glass surface was calculated using the following method. The four normal force transducers were summed. The impact spot area was extracted as a function of time using image analysis of the high-speed video. The pressure was then calculated by dividing the net force by the extracted spot area.

This method was used to analyze EDC37 drops at an incident angle of 14° at 9 ft (Drop 563) and 6 ft (Drop 561) drop heights. These data were compared to a 6 ft PBX 9501 drop at an incident angle of 14° (Drop 564). The normal force traces for these drops is shown in Figure 24, Figure 25, and Figure 26. The lateral force data for these drops are compared in Figure 28. The spot areas and calculated pressures are compared in Figure 27. Note that the spot area for the EDC37 was almost twice the area of the PBX 9501 on the 6 ft drop, while the net peak force during all three of these highlighted experiments was the same, ~14 kN. The pressures attained on both the 6 ft and the 9 ft EDC37 drops were significantly lower than the 6 ft PBX 9501 impact pressure.

However, note that the peak pressure reached during the 6 ft EDC37 drop is higher than the 9 ft drop, which is counterintuitive. We believe this originates from problems with the method of obtaining a net force from the four individual force transducers. Note the lack of synchrony in the individual force traces in Drop 561, EDC37 6 ft (Figure 25), in comparison with Drop 563 (Figure 24) and Drop 564 (Figure 26). It is observed that the peak lateral force in Drop 563 and Drop 564 line up with their correlated peak impact times (Figure 28). However, the lateral force in Drop 561 reduces significantly at its peak impact time, which could explain the inconsistent normal force data in Figure 25. The sample may also have impacted slightly off-center, in comparison. Whatever the source of the error, the lateral force transducer suggests that the net force (and pressure) calculated for Drop 561 is less reliable than the other two drops. We acknowledge problems with the method, but are currently unaware of a superior method for estimating the pressure attained during the impact.

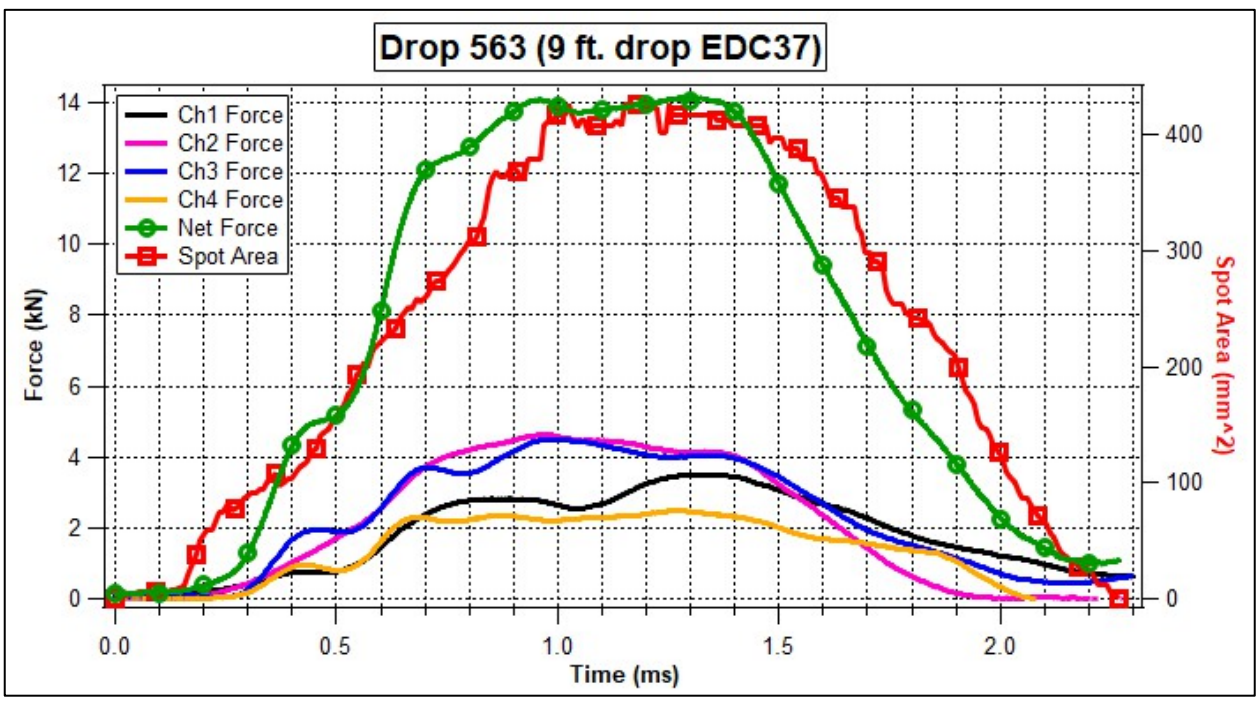

Figure 24. Data of force acting on the target plate and measured pressure spot area on EDC37 for Drop 563.

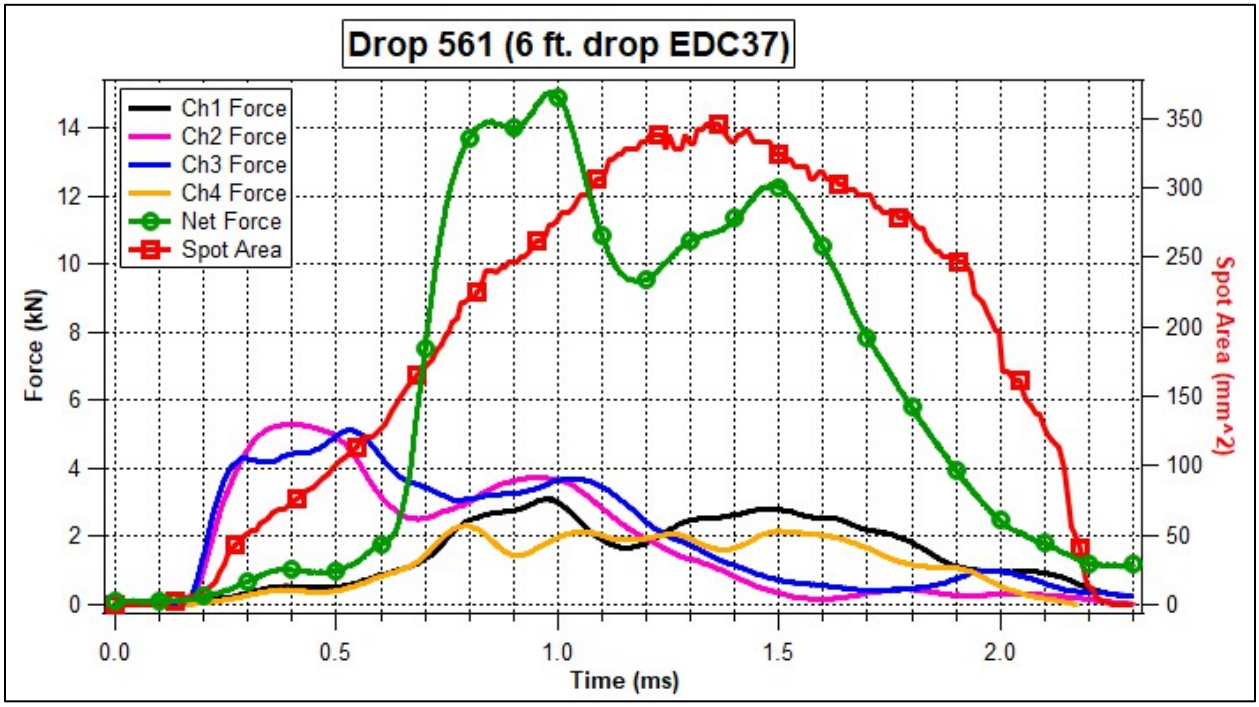

Figure 25. Data of force acting on the target plate and measured pressure spot area on EDC37 for Drop 561.

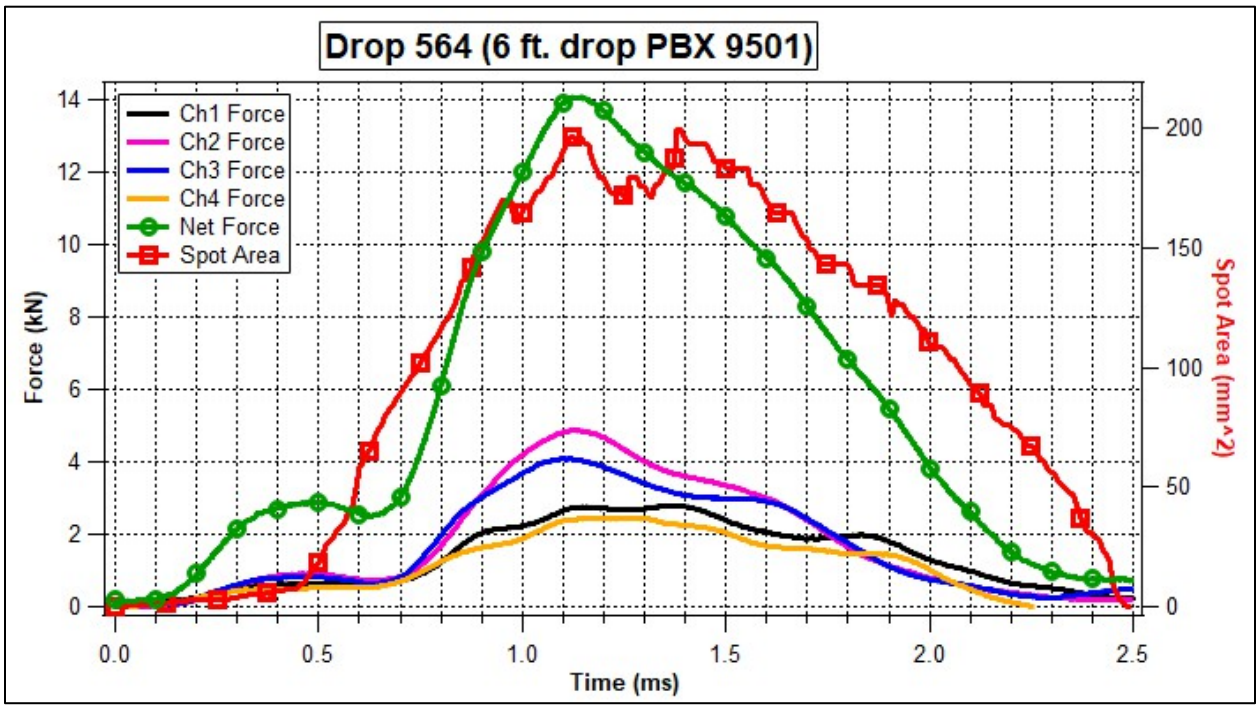

Figure 26. Data of force acting on the target plate and measured pressure spot area on PBX 9501 for Drop 564.

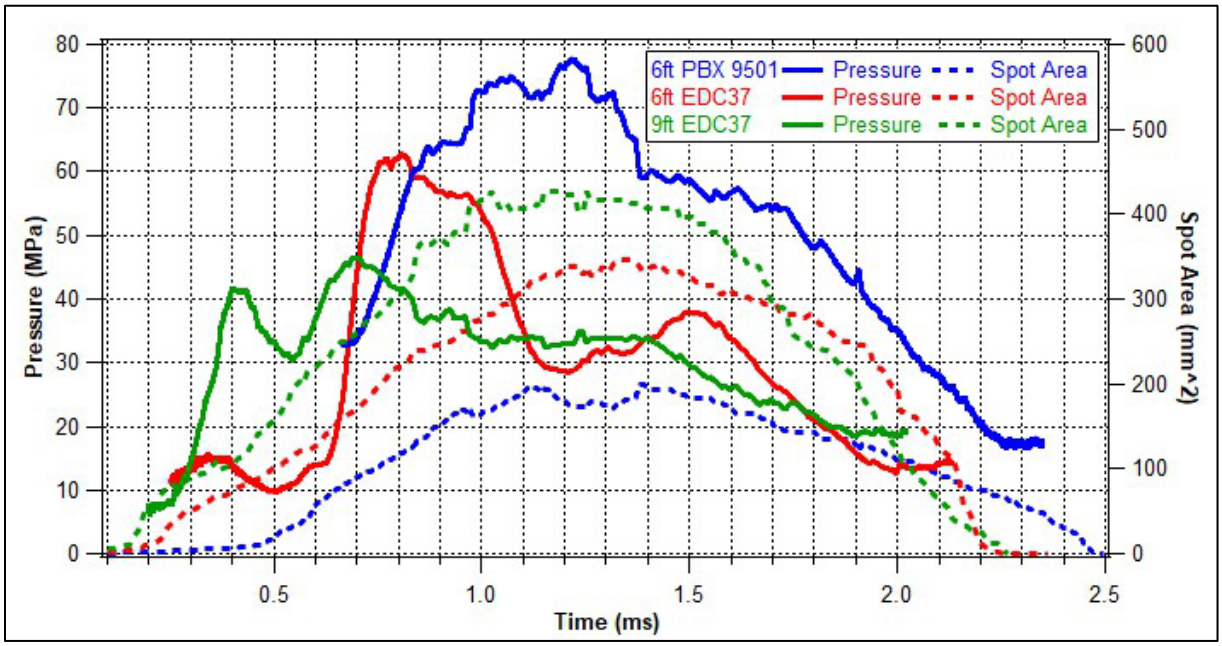

Figure 27. Pressure and spot area comparison for Drops 561, 563, and 564.

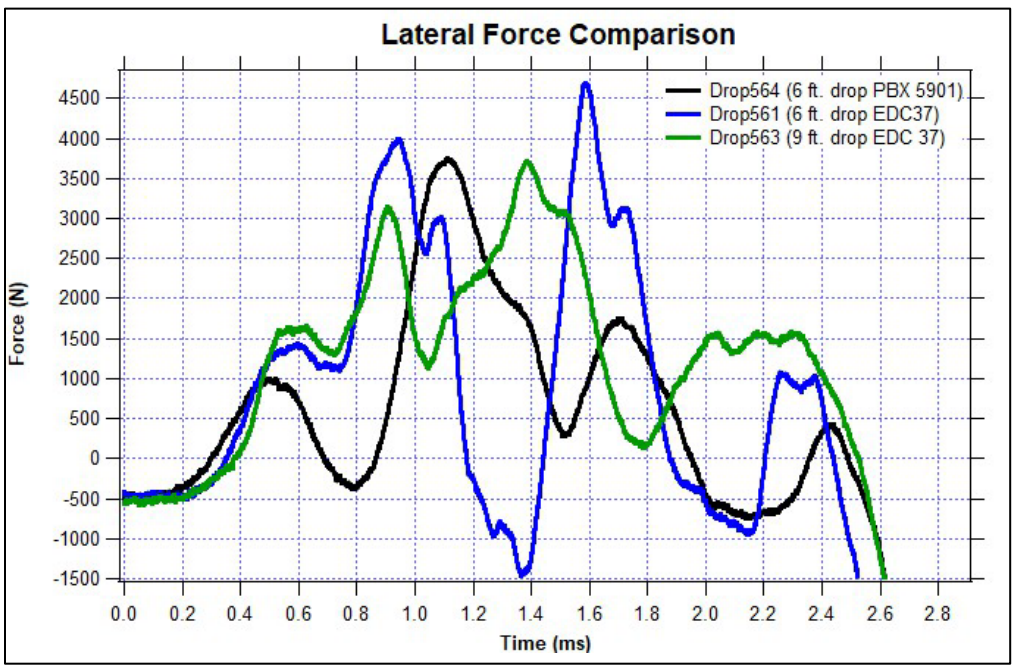

Figure 28. Lateral Fore Comparison for Drop564, Drop561, and Drop563. Notice the decrease in force at 1.2 ms for Drop561.

The pressure attained during impact is relevant to the explosive response. The amount of frictional heating available to generate a hot spot is proportional to the normal force applied to the grit particle. The normal force applied to the grit particle is affected by the net contact spot pressure as well as the indentation hardness of the explosive surface. EDC37 exhibits a lower indentation hardness than PBX 9501 on the Shore D scale (Table 3). EDC37 also has a lower compressive strength than PBX 9501 [27,28], and this is reflected in the considerably larger spot area observed during Skid Test impacts. The lower indentation hardness and lower average contact pressure cause a lower normal force to be applied to the grit particle, thereby reducing the frictional heating of EDC37 relative to PBX 9501.

6. Conclusions

Thirty-one Skid Tests were performed in the study of grit-grit interactions among PBX 9501. An explosive charge with pre-embedded grit was dropped onto a gritty Adiprene polymer surface, at a range of impact angles and grit sizes. The grit size embedded in the HE remained constant. All drops were performed with an equivalent drop height of 6 ft. No ignition was observed in any of the grit-grit interaction drops.

Previously, it had been hypothesized that the source of reaction mitigation when impacting soft rubber targets was the preferential embedding of grit entirely into the rubber, thus preventing grit-grit impacts. These new data suggest an updated hypothesis: despite grit-grit impacts, no ignitions are observed on soft rubber targets because the normal force applied to a grit particle by the rubber is insufficient to provide the frictional heating necessary for ignition. Regardless the cause, the effect of a soft rubber target material remains the same: ignitions are mitigated. Thus the previously supplied guidance to use protective mats with hardness ≤ 40 (Shore D) remains valid [15].

Eleven tests were conducted with EDC37 impacting gritty glass at a range of drop heights, impact angles, and grit sizes. In this series, a single test (Drop 563) resulted in ignition, at a drop height of 9 ft and incident angle of 14˚. Hot spots were observed to form and quench, with no additional violence. In comparison with equivalent drops on PBX 9501 that we reported in previous years, EDC37 is less prone to explosive ignition and reaction in these sorts of low-velocity frictional impact insults.

In previous skid testing, it was observed that the material properties of the explosive composition had an effect on the post-ignition violence, but not on the pre-ignition behavior (different compositions exhibited hotspot ignitions at statistically indistinguishable drop heights, and differences in response only emerged in the post-ignition regime of response). With the latest EDC37 tests, we observed that composition also has an effect on whether or not ignitions occur in the first place.

Force and contact spot area were analyzed to calculate the pressure attained between the HE and impact surface. The contact pressure for EDC37 was found to be less than a PBX 9501 drop with similar parameters. We hypothesize that the reduced contact pressure as well as the lower hardness of EDC37 (compared to PBX 9501) serve to reduce the frictional heating that is delivered to grit particles during the impact event, thus mitigating explosive reaction.

7. Future Work

This year's results highlighted the role of explosive hardness in frictional heating on grit contaminated surfaces. It has been observed in previous Skid Testing that compositions with identical fill-fractions of HMX exhibit differing post-ignition response. Now we see an effect on the pre-ignition response as well. This was observed for LX-14 (5% Estane), LX-10 (5% Viton), and PBX 9501(2.5%Estane, 2.5%BDNPA/F) [20]. This implicates the binder as the culprit (thought we note that differences in the crystal size distribution of HMX may also affect hardness). Estane and Viton differ in their nominal hardness, and the BDNPA/F plasticizer added to PBX 9501 will reduce the hardness of the Estane.

Additionally, polymer hardness varies with temperature. The frictional heating must produce temperatures in excess of 500˚C in order to ignite the HMX within the timescale of the impact event [29]. As the polymer is heated to this ignition temperature, the thermal variation of the polymer hardness may affect the frictional normal force, and thus explosive response. In this sense, the propensity for a binder to easily soften with elevated temperature may help mitigate ignition. The hypothetical scenario would progress as follows: as the grit particle heats the explosive on the path to ignition, the elevated temperature softens the binder, which reduces the normal force, dampens the frictional heating source, and mitigates the ignition. If this scenario is accurate, it is somewhat ironic: thermal stability of a binder system is generally considered a positive safety attribute, particularly in the context of cookoff insult scenarios [30]. However, in the context of a grit-mediated frictional ignition, thermal stability of the binder may help sustain hardness to higher temperatures, thereby allowing sufficient frictional normal force to provide an ignition mechanism. Further research is warranted on the issue of binder hardness, and the hardness as a function of temperature for different binder systems. Additionally, a study in which the binder hardness is controlled as an independent variable would

provide valuable data regarding the particular material attributes of explosives that are responsible for ignition in an oblique impact.

As mentioned, the radius of curvature of the Shore D indenter (100 μm) is on the same length scale as the HMX crystal size of PBX 9501 (234 μm). Consequently, the Shore D hardness of an explosive composition may be an ideal measurement to probe the mesoscale properties of the explosive that are most relevant in determining explosive response. In the effort to predict explosive response, it will be necessary to develop a constitutive mechanical model that is valid on the mesoscale. Measurements of Shore D hardness, and the way in which hardness varies as a function of temperature and composition, may prove an ideal dataset against which to validate a constitutive model that accurately captures the mesoscale regime.

8. Acknowledgments

We gratefully acknowledge funding from Paul Peterson through the NSR&D program.

9. Data Requests

Videos of the tests as well as various other raw data can be made available on request. Please contact Matt Holmes at mholmes@lanl.gov or 505-665-4107.

10. References

[1] Smith, L. C. and Popolato, A., "Summary of Discussions with British, JOWOG-9, 22-24 June 1959", Memorandum, *Los Alamos Scientific Laboratory*, October 23, 1959.
[2] Skidmore, C. B., "Photographs Related to the Burning Ground Accident in 1959" *Los Alamos National Laboratory Report: LA-UR-13-21811*, 2013.
[3] Personal Communication, From: Fleming, K., To: C. B. Skidmore, Friday, October 16, 2015, 4:59:39AM.
[4] Fleming, K., "Documents associated with an accident at AWRE in 1959", Memorandum, *AWRE*, October, 2015.
[5] Brawley, E. L., Brooks, M. L., Courtright, W. C., Drake, R. W. and Reider, R., "Explosion at S-Site on February 24, 1959" *Los Alamos National Laboratory* 1959.
[6] Parker, G., Holmes, M., Heatwole, E., Vaughan, L. and Dickson, P., "Friction-induced heating and ignition of PBX 9501" *Proceedings of the Fifteenth International Detonation Symposium*, pp. 1536-1542, San Francisco, CA, 2014.
[7] Dickson, P., Parker, G. and Novak, A., "Frictionally Induced Ignition Processes in Drop and Skid Tests" *Proceedings of the 14th International Detonation Symposium*, pp. 952-959, Coeur d'Alene, ID, 2010.
[8] Holmes, M. D., Rae, P. J., Haroz, E. H. and Erickson, M. A., "Shear Heating of Explosives using the Crush Gun; FY2018 Report" *Los Alamos National Laboratory Report: LA-UR-18-30889*, 2018.
[9] Holmes, M. D., Rae, P. and Parker, G. R., "Viscous Heating via Low-Velocity Crushing Impact of High Explosives" *Proceedings of the 16th International Detonation Symposium*, Cambridge, MD, 2018.
[10] Dyer, A. S. and Taylor, J. W., "Initiation of Detonation by Friction on a High Explosive Charge" *Proceedings of the 5th Internation Detonation Symposium*, pp. 291-300, Pasadena, CA, 1970.
[11] Slape, R. J., "IHE Material Qualification Test Description and Criteria", 1984
[12] Hayden, D. J., "An Analytic Tool to Investigate the Effect of Binder on the Sensitivity of HMX-Based Plastic Bonded Explosives in the Skid Test", Type of Work, Report 2004
[13] Randolph, A. D., "Recent Progress in the Large-Scale Skid Sensitivity Test" *Report: LA-5122-MS*, 1972.
[14] Parker, G. R., Heatwole, E. M., Holmes, M. D., Gunderson, J. A., Novak, A. M., et al., "The Effect of Grit on Frictional Heating During Oblique Impacts with PBX 9501" *Los Alamos National Laboratory Report: LA-UR-13-25703*, 2013.
[15] Parker, G. R. J., Heatwole, E. M., Holmes, M. D., Vaughan, L. D. and Dickson, P., "The Effect of Grit on Frictional Heating During Oblique Impacts with PBX 9501 Fiscal Year 2014 Update" *Los Alamos National Laboratory Report: LA-UR-14-27843*, 2014.
[16] Heatwole, E. M., Parker, G. R., Holmes, M. D. and Dickson, P., "Grit-mediated frictional ignition fo a polymer-bonded explosive during oblique impacts: Probability calculations for safety engineering" *Reliability Engineering and System Safety,* Vol. 134, pp. 10-18, 2015.
[17] Parker, G. R., Holmes, M. D., Heatwole, E. M. and Vaughan, L. D., "Oblique Impacts with PBX 9501: Fiscal Year 2015 Skid Testing Results" *Los Alamos National Laboratory Report: LA-UR-15-27394*, 2015.
[18] Parker, G. R. J., Holmes, M. D., Heatwole, E. M., Vaughan, L. D., Broilo, R. M., et al., "Oblique Impacts with PBX 9404, LX-14, LX-10 and Aged PBX 9501" *Los Alamos National Laboratory Report: LA-UR-16-26795*, 2016.

[19] Broilo, R. M., Parker, G. R., Lopez-Pulliam, I. D., Vaughan, L. D., Holmes, M. D., et al., "Oblique Impacts with PBX 9501, PBX 9407, Comp B and Naturally Aged PBX 9501 Hemi Shells" *Los Alamos National Laboratory Report: LA-CP-18-20109*, 2018.
[20] Broilo, R. M., Parker, G. R., Holmes, M. D., Lopez-Pulliam, I. D. and Heatwole, E. M., "Magnitude of Response to Frictional Ignition by Oblique Impact of High Explosives Formulations" *16th International Detonation Symposium*, Vol. 2018.
[21] International, A., "ASTM D2240", 2017
[22] Skidmore, C. B., Phillips, D. S., Son, S. F. and Asay, B. W., "Characterization of HMX Particles in PBX 9501" *Proceedings of the Shock Compression of Condensed Matter*, 10.1063/1.55666, 1997.
[23] Skidmore, C. B., Phillips, D. S., Howe, P. M., Mang, J. T. and Romero, J. A., "The evolution of microstructural changes in pressed HMX explosives" *11th International Detonation Symposium*, Vol. 10.2172/334323, 1998.
[24] Burch, A. C., Yeager, J. D. and Bahr, D. F., "Nanoindentation of HMX and Idoxuridine to Determine Mechanical Similarity" *Crystals,* Vol. 7, 10.3390/cryst7110335, 2017.
[25] Yeager, J. D., Watkins, E. B., Duque, A. L. and Majewski, J., "The Thermal and Microstructural Effect of Plasticizing HMX-Nitrocellulose Composites" *Journal of Energetic Materials,* Vol. 36, pp. 13-28, 10.1080/07370652.2017.1301597, 2017.
[26] Olinger, B., "Compacting Plastic-Bonded Explosive Molding Powders to Dense Solids" *Los Alamos National Laboratory Report: LA-14173*, 2005.
[27] Williamson, D. M., Siviour, C. R., Proud, W. G., Palmer, S. J. P., Govier, R., et al., "Temperature-time response of a polymer bonded explosive in compression (EDC37)" *Journal of Applied Physics D.,* Vol. 41, 10.1088/0022-3727/41/8/085404, 2008.
[28] Govier, R. K., Gray III, G. T. and Blumenthal, W. R., "Comparison of the Influence of Temperature on the High-Strain-Rate Mechanical Responses of PBX 9501 and EDC37" *Metallurgical and Materials Transactions A,* Vol. 39A, pp. 535-538, 10.1007/s11661-007-9430-0, 2008.
[29] Henson, B., Asay, B. W., Smilowitz, L. B. and Dickson, P., "Ignition chemistry in HMX from thermal explosion to detonation" *Proceedings of the Shock Compression of Condensed Matter*, pp. 1069-1072, 2001.
[30] Parker, G. R., Dickson, P., Asay, B. W. and McAfee, J. M., "DDT of Hot, Thermally Damaged PBX 9501 in Heavy Confinement" *Proceedings of the 14th International Detonation Symposium*, pp. 941-951, Coeur d'Alene, ID, 2010.

Appendix A: FY 19 Test Record

Day	Drop # (daily)	Drop # (remote log)	Date	Time of Drop	Angle of Impact	HI Type	HI Model	Material HI?	Drop Angle (from vertical, degrees)	HI Drop Height (from freeboard)	Nominal Height	Shape of HI Strike	Dunnage in Advance	EPS Cut	EPS Size	Adhesive Type	Final Image Video Name	Final Image Frame File (proof of process in GIF)	Lens Aperture	HI Cinema File Name	Image Data File Name	Lid Off	Crush Start	Drop Start	Quick Note Impressions
1	1	534	09/26/19	9:13:45	45°	EDC 37	7378L	N	44.39°	6' 11"	9"	chamfered plate	N/A	N/A	N/A	higher velocity	Drop534_dual.avi	1100000ppm 3psi 98kPa 30000 5.0psi 70lbf=769	f/1.1	6750.JPG	Snapat1_here	N	N	N	No anomalies
1	2	535	09/26/19	9:43:45	45°	EDC 37	7378L	N	34.95°	9.6"	9"	rounded plate	N/A	2	3.5-5.5lbs	higher velocity	Drop535_dual.avi	1100000ppm 3psi 98kPa 30000 5.0psi 70lbf=770	f/1.3	6755.JPG	Snapat1_here	N	N	N	Small dimple bottom
1	3	536	09/26/19	10:46:45	45°	EDC 37	7378L	N	35.15°	9.8"	9"	rounded plate	N/A	2	3.5-5.5lbs	higher velocity	Drop536_dual.avi	1100000ppm 3psi 98kPa 30000 5.0psi 70lbf=771	f/1.3	6760.JPG	Snapat1_here	N	N	N	No anomalies
1	4	537	09/26/19	10:16:45	45°	EDC 37	7378L	N	44.38°	6' 8.5"	6'	rounded plate	N/A	2	3.5-5.5lbs	higher velocity	Drop537_dual.avi	1100000ppm 3psi 98kPa 30000 5.0psi 70lbf=772	f/1.4	6765.JPG	Snapat1_here	N	N	N	No anomalies
1	5	538	09/26/19	10:41:45	45°	EDC 37	7378L	N	44.85°	6' 8.5"	6'	rounded plate	N/A	2	3.5-5.5lbs	higher velocity	Drop538_dual.avi	1100000ppm 3psi 98kPa 30000 5.0psi 70lbf=773	f/1.5	6770.JPG	Snapat1_here	N	N	N	No anomalies
1	6	539	09/26/19	11:46:45	45°	EDC 37	7378L	N	44.55°	6' 13"	6'	rounded plate	N/A	1	0.5-1lbs	higher velocity	Drop539_dual.avi	1100000ppm 3psi 98kPa 30000 5.0psi 70lbf=774	f/1.6	6775.JPG	Snapat1_here	N	N	N	No anomalies
1	7	540	09/26/19	12:34:45	45°	EDC 37	7378L	N	44.17°	6' 8.5"	6'	rounded plate	N/A	3	5.5-25lbs	higher velocity	Drop540_dual.avi	1100000ppm 3psi 98kPa 30000 5.0psi 70lbf=775	f/1.7	6780.JPG	Snapat1_here	N	N	N	No anomalies
1	8	541	09/26/19	13:44:45	45°	EDC 37	7378L	N	43.97°	6' 8.8"	6'	rounded plate	N/A	4	25-150lbs	higher velocity	Drop541_dual.avi	1100000ppm 3psi 98kPa 30000 5.0psi 70lbf=776	f/1.8	6785.JPG	Snapat1_here	N	N	N	No anomalies
1	9	542	09/26/19	14:56:45	45°	PKG 5581 bowtie	7378L	N	44.18°	6' 11"	6'	required adjusted D44 block	41	1	0.5lbs	higher velocity	Drop542_dual.avi	1100000ppm 3psi 98kPa 30000 5.0psi 70lbf=777	f/1.9	6790.JPG	Snapat1_here	N	N	N	No anomalies
2	1	543	09/26/19	9:53:45	45°	PKG 5581 bowtie	7378L	N	44.51°	6' 13"	6'	required adjusted D45 dunnage	46	1	0.5lbs	higher velocity	Drop543_non-video.dat	1100000ppm 3psi 98kPa 30000 5.0psi 70lbf=778	f/1.8	6795.JPG	Snapat1_here	N	N	N	No anomalies
2	2	544	09/26/19	10:46:45	45°	PKG 5581 bowtie	7378L	N	44.31°	6' 8.9"	6'	required adjusted D44 block	48	1	0.5lbs	higher velocity	Drop544_dual.avi	1100000ppm 3psi 98kPa 30000 5.0psi 70lbf=779	f/1.8	6800.JPG	Snapat1_here	N	N	N	No anomalies
2	3	545	09/26/19	11:38:45	45°	PKG 5581 bowtie	7378L	N	N/A	6' 8.5"	6'	required adjusted D44 block	48	1	0.5lbs	higher velocity	Drop545_dual.avi	1100000ppm 3psi 98kPa 30000 5.0psi 70lbf=780	f/1.9	6805.JPG	Snapat1_here	N	N	N	No anomalies
2	4	546	09/26/19	12:58:45	45°	PKG 5581 bowtie	7378L	N	N/A	6' 8.7"	6'	required adjusted D44 block	44	1	0.5lbs	higher velocity	Drop546_non-video.dat	1100000ppm 3psi 98kPa 30000 5.0psi 70lbf=781	f/1.8	6810.JPG	Snapat1_here	N	N	N	No anomalies
2	5	547	09/26/19	11:13:45	45°	PKG 5581 bowtie	7378L	N	N/A	6' 13"	6'	required adjusted D44 block	48	1	0.5lbs	higher velocity	Drop547_dual.avi	1100000ppm 3psi 98kPa 30000 5.0psi 70lbf=782	f/1.8	6815.JPG	Snapat1_here	N	N	N	No anomalies
2	6	548	09/26/19	11:37:45	45°	PKG 5581 bowtie	7378L	N	N/A	6' 14"	6'	required adjusted D44 block	48	2	3.5-5.5lbs	higher velocity	Drop548_dual.avi	1100000ppm 3psi 98kPa 30000 5.0psi 70lbf=783	f/1.9	6820.JPG	Snapat1_here	N	N	N	No anomalies
2	7	549	09/26/19	11:50:45	45°	PKG 5581 bowtie	7378L	N	N/A	6' 8.8"	6'	required adjusted D44 block	48	3	5.5-25lbs	higher velocity	Drop549_dual.avi	1100000ppm 3psi 98kPa 30000 5.0psi 70lbf=784	f/1.6	6825.JPG	Snapat1_here	N	N	N	No anomalies
2	8	550	09/26/19	12:09:45	45°	PKG 5581 bowtie	7378L	N	N/A	6' 18"	6'	required adjusted D44 block	48	4	25-150lbs	higher velocity	Drop550_non-video.dat	1100000ppm 3psi 98kPa 30000 5.0psi 70lbf=785	f/1.7	6830.JPG	Snapat1_here	N	N	N	No anomalies
2	9	551	09/26/19	12:19:45	45°	PKG 5581 bowtie	7378L	N	N/A	6' 8.8"	6'	rounded adjusted D55 gray	37	1	0.5lbs	higher velocity	Drop551_non-video.dat	1100000ppm 3psi 98kPa 30000 5.0psi 70lbf=786	f/1.8	6835.JPG	Snapat1_here	N	N	N	No anomalies
2	10	552	09/26/19	13:17:45	45°	PKG 5581 bowtie	7378L	N	N/A	6' 8.8"	6'	rounded adjusted D55 gray	37	1	0.5lbs	higher velocity	Drop552_dual.avi	1100000ppm 3psi 98kPa 30000 5.0psi 70lbf=787	f/1.9	6840.JPG	Snapat1_here	N	N	N	No anomalies
2	11	553	09/26/19	13:27:45	45°	PKG 5581 bowtie	7378L	N	N/A	6' 8.8"	6'	required adjusted D44 block	41	2	3.5-5.5lbs	higher velocity	Drop553_non-video.dat	1100000ppm 3psi 98kPa 30000 5.0psi 70lbf=788	f/1.8	6845.JPG	Snapat1_here	N	N	N	No anomalies
2	12	554	09/26/19	13:34:45	45°	PKG 5581 bowtie	7378L	N	N/A	6' 8.9"	6'	required adjusted D44 block	48	2	3.5-5.5lbs	higher velocity	Drop554_non-video.dat	1100000ppm 3psi 98kPa 30000 5.0psi 70lbf=789	f/1.9	6850.JPG	Snapat1_here	N	N	N	No anomalies
2	13	555	09/26/19	13:43:45	45°	PKG 5581 bowtie	7378L	N	N/A	6' 8.8"	6'	required adjusted D44 block	59	2	3.5-5.5lbs	higher velocity	Drop555_non-video.dat	1100000ppm 3psi 98kPa 30000 5.0psi 70lbf=790	f/1.8	6855.JPG	Snapat1_here	N	N	N	No anomalies
2	14	556	09/26/19	13:59:45	45°	PKG 5581 bowtie	7378L	N	N/A	6' 8.8"	6'	required adjusted D44 block	59	2	3.5-5.5lbs	higher velocity	Drop556_non-video.dat	1100000ppm 3psi 98kPa 30000 5.0psi 70lbf=791	f/1.8	6860.JPG	Snapat1_here	N	N	N	No anomalies
2	15	557	09/26/19	14:38:45	45°	PKG 5581 bowtie	7378L	N	N/A	6' 14"	6'	required adjusted D44 block	59	2	3.5-5.5lbs	higher velocity	Drop557_dual.avi	1100000ppm 3psi 98kPa 30000 5.0psi 70lbf=792	f/1.8	6865.JPG	Snapat1_here	N	N	N	No anomalies
2	16	558	09/26/19	14:17:45	45°	PKG 5581 bowtie	7378L	N	N/A	6' 16"	6'	required adjusted D44 block	59	2	3.5-5.5lbs	higher velocity	Drop558_dual.avi	1100000ppm 3psi 98kPa 30000 5.0psi 70lbf=793	f/1.5	6870.JPG	Snapat1_here	N	N	N	No anomalies
3	1	559	09/26/19	9:47:45	45°	PKG 5581	7378L	N	44.44°	6' 13"	6'	dual dunnage block, adhered	N/A	N/A	N/A	higher velocity	Drop559_non-video.dat	1100000ppm 3psi 98kPa 30000 5.0psi 70lbf=794	f/1.6	6875.JPG	Snapat1_here	N	N	N	No anomalies
3	2	560	09/26/19	10:41:45	45°	EDC 37	7378L	N	55.62°	9' 11"	9'	rounded plate	N/A	2	3.5-5.5lbs	higher velocity	Drop560_non-video.dat	1100000ppm 3psi 98kPa 30000 5.0psi 70lbf=795	f/1.7	6880.JPG	Snapat1_here	N	N	N	No anomalies

3	3	561	10/16/19	11:08	14°	ETC 37	71785	N	44.11°	6' 8.6"	6'	sanded glass	N/A	2	15.8-5.8kpa	hopper water	Drop561_dassell.csv Drop561_overview.csv	11.000kpa Tyn 914-384 10000 5kpa 762x796	116 10.38	7819.JPG - 7883.JPG	Scope1_force Scope2_lm_force_and_timing_bind/Drop561	N	N	N	No motion
3	4	562	10/16/19	11:18	14°	ETC 37	71785	N	55.59°	9' 1.9"	9'	sanded glass	N/A	2	15.8-5.8kpa	hopper water	Drop562_dassell.csv Drop562_overview.csv	11.000kpa Tyn 914-384 10000 5kpa 762x797	116 10.39	7883.JPG - 7850.JPG	Scope1_force Scope2_lm_force_and_timing_bind/Drop562	N	N	N	No motion
3	5	563	10/16/19	11:31	14°	ETC 37	71785	N	55.86°	9' 8.7"	9'	sanded glass	N/A	1	>5.8kpa	hopper water	Drop563_dassell.csv Drop563_overview.csv	11.000kpa Tyn 914-384 10000 5kpa 762x798	116 10.38	7851.JPG - 7862.JPG	Scope1_force Scope2_lm_force_and_timing_bind/Drop563	Y	N	N	Sparkles
3	6	564	10/16/19	11:46	14°	PRV 15.81	71698	N	N/A	6' 1.6"	6'	sanded glass	N/A	1	>5.8kpa	hopper water	Drop564_dassell.csv Drop564_overview.csv	11.000kpa Tyn 914-384 10000 5kpa 762x799	116 10.31	7863.JPG - 7881.JPG	Scope1_force Scope2_lm_force_and_timing_bind/Drop564	Y	N	N	Sparkles
4	1	565	10/18/19	8:01	14°	PRV 15.81 Sanded	71698	N	44.37°	6' 8.9"	6'	sanded glass	39	1	>5.8kpa	hopper water	Drop565_dassell.csv Drop565_overview.csv	11.000kpa Tyn 914-384 10000 5kpa 762x800	116 10.32	7882.JPG - 7113.JPG	Scope1_force Scope2_lm_force_and_timing_bind/Drop565	N	N	N	No motion
4	2	566	10/18/19	8:19	14°	PRV 15.81 Sanded	71698	N	44.89°	6' 8.5"	6'	sanded glass	39	1	>5.8kpa	hopper water	Drop566_dassell.csv Drop566_overview.csv	11.000kpa Tyn 914-384 10000 5kpa 762x801	116 10.33	7114.JPG - 7119.JPG	Scope1_force Scope2_lm_force_and_timing_bind/Drop566	N	N	N	No motion
4	3	567	10/18/19	8:38	14°	PRV 15.81 Sanded	71698	N	44.11°	6' 8.6"	6'	sanded glass	41	1	>5.8kpa	hopper water	Drop567_dassell.csv Drop567_overview.csv	11.000kpa Tyn 914-384 10000 5kpa 762x802	116 10.34	7118.JPG - 7127.JPG	Scope1_force Scope2_lm_force_and_timing_bind/Drop567	N	N	N	No motion
4	4	568	10/18/19	8:48	14°	PRV 15.81 Sanded	71698	N	44.48°	6' 1.7"	6'	sanded glass	39	1	>5.8kpa	hopper water	Drop568_dassell.csv Drop568_overview.csv	11.000kpa Tyn 914-384 10000 5kpa 762x803	116 10.35	7128.JPG - 7135.JPG	Scope1_force Scope2_lm_force_and_timing_bind/Drop568	N	N	N	No motion
4	5	569	10/18/19	8:53	14°	PRV 15.81 Sanded	71698	N	44.93°	6' 1.3"	6'	sanded glass	39	1	>5.8kpa	hopper water	Drop569_dassell.csv Drop569_overview.csv	11.000kpa Tyn 914-384 10000 5kpa 762x804	116 10.36	7136.JPG - 7143.JPG	Scope1_force Scope2_lm_force_and_timing_bind/Drop569	N	N	N	No motion
4	6	570	10/18/19	9:02	14°	PRV 15.81 Sanded	71698	N	44.13°	6' 8.7"	6'	sanded glass	39	1	>5.8kpa	hopper water	Drop570_dassell.csv Drop570_overview.csv	11.000kpa Tyn 914-384 10000 5kpa 762x805	116 10.37	7143.JPG - 7150.JPG	Scope1_force Scope2_lm_force_and_timing_bind/Drop570	N	N	N	No motion
4	7	571	10/18/19	9:16	14°	PRV 15.81 Sanded	71698	N	44.15°	6' 8.7"	6'	sanded glass	39	2	15.8-5.8kpa	hopper water	Drop571_dassell.csv Drop571_overview.csv	11.000kpa Tyn 914-384 10000 5kpa 762x806	116 10.38	7151.JPG - 7157.JPG	Scope1_force Scope2_lm_force_and_timing_bind/Drop571	N	N	N	No motion
4	8	572	10/18/19	9:37	14°	PRV 15.81 Sanded	71698	N	44.18°	6' 8.5"	6'	sanded glass	39	2	15.8-5.8kpa	hopper water	Drop572_dassell.csv Drop572_overview.csv	11.000kpa Tyn 914-384 10000 5kpa 762x807	116 10.39	7158.JPG - 7165.JPG	Scope1_force Scope2_lm_force_and_timing_bind/Drop572	N	N	N	No motion
4	9	573	10/18/19	9:49	14°	PRV 15.81 Sanded	71698	N	44.14°	6' 8.6"	6'	sanded glass	39	2	15.8-5.8kpa	hopper water	Drop573_dassell.csv Drop573_overview.csv	11.000kpa Tyn 914-384 10000 5kpa 762x808	116 10.40	7166.JPG - 7173.JPG	Scope1_force Scope2_lm_force_and_timing_bind/Drop573	N	N	N	No motion
4	10	574	10/18/19	10:00	14°	PRV 15.81 Sanded	71698	N	44.80°	6' 8.4"	6'	sanded glass	39	2	15.8-5.8kpa	hopper water	Drop574_dassell.csv Drop574_overview.csv	11.000kpa Tyn 914-384 10000 5kpa 762x809	116 10.41	7174.JPG - 7181.JPG	Scope1_force Scope2_lm_force_and_timing_bind/Drop574	N	N	N	No motion
4	11	575	10/18/19	10:09	14°	PRV 15.81 Sanded	71698	N	44.95°	6' 8.8"	6'	sanded glass	39	2	15.8-5.8kpa	hopper water	Drop575_dassell.csv Drop575_overview.csv	11.000kpa Tyn 914-384 10000 5kpa 762x810	116 10.42	7182.JPG - 7190.JPG	Scope1_force Scope2_lm_force_and_timing_bind/Drop575	N	N	N	No motion
4	12	576	10/18/19	10:19	14°	PRV 15.81 Sanded	71699	N	N/A	6' 8.8"	6'	sanded glass	39	2	15.8-5.8kpa	hopper water	Drop576_dassell.csv Drop576_overview.csv	11.000kpa Tyn 914-384 10000 5kpa 762x811	116 10.43	7191.JPG - 7196.JPG	Scope1_force Scope2_lm_force_and_timing_bind/Drop576	N	N	N	No motion
4	13	577	10/18/19	10:39	14°	PRV 15.81 Sanded	71699	N	43.97°	6' 8.9"	6'	sanded glass	39	5	15.8-25kpa	hopper water	Drop577_dassell.csv Drop577_overview.csv	11.000kpa Tyn 914-384 10000 5kpa 762x812	116 10.44	7197.JPG - 7206.JPG	Scope1_force Scope2_lm_force_and_timing_bind/Drop577	N	N	N	No motion
4	14	578	10/18/19	10:39	14°	PRV 15.81 Sanded	71699	N	44.36°	6' 1.6"	6'	sanded glass	39	4	75-15kpa	hopper water	Drop578_dassell.csv Drop578_overview.csv	11.000kpa Tyn 914-384 10000 5kpa 762x813	116 10.45	7207.JPG - 7210.JPG	Scope1_force Scope2_lm_force_and_timing_bind/Drop578	N	N	N	No motion

Appendix B: CAD Illustrations of the Pendulum Apparatus

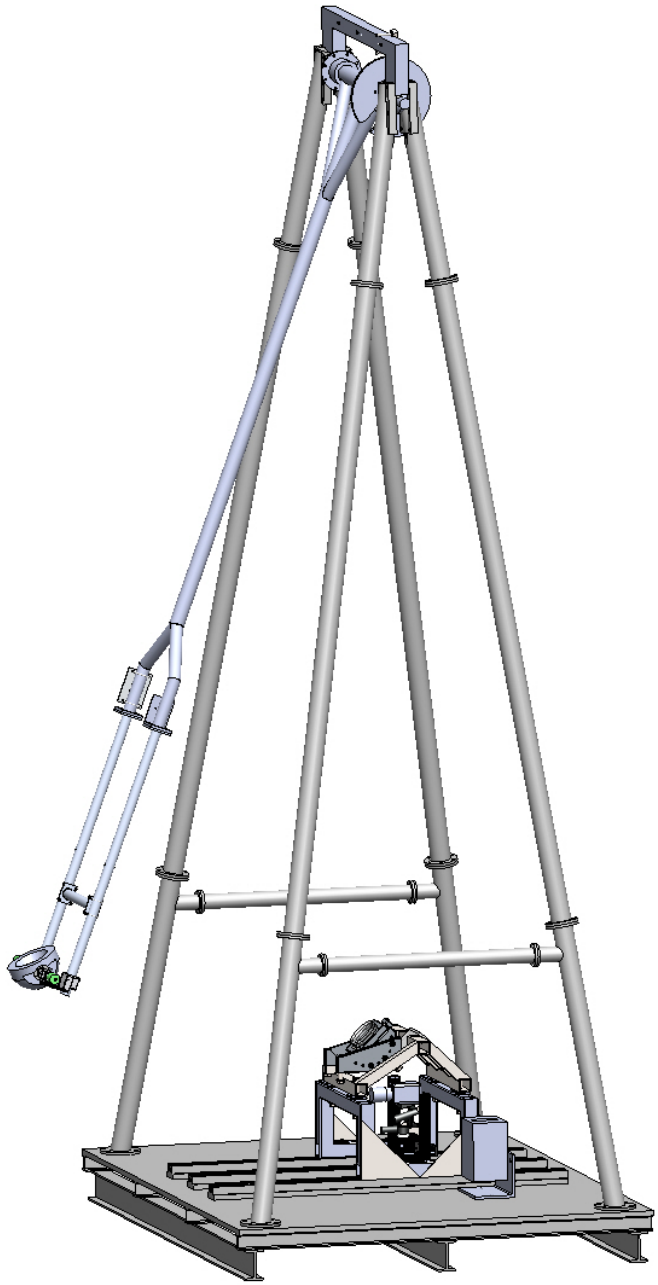

Figure 29. CAD pendulum angle view.

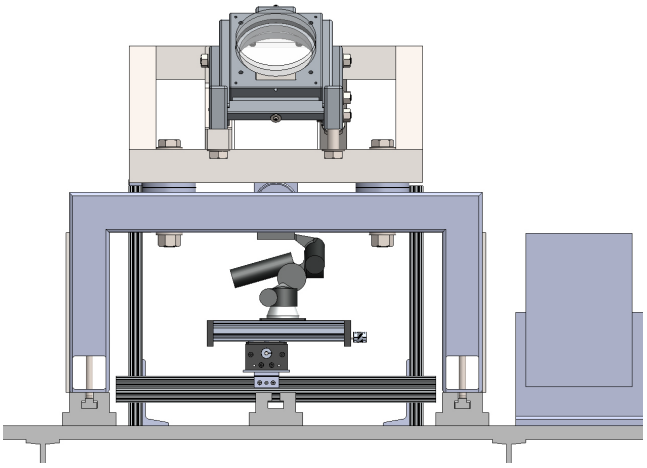

Figure 30. CAD front view of target frame.

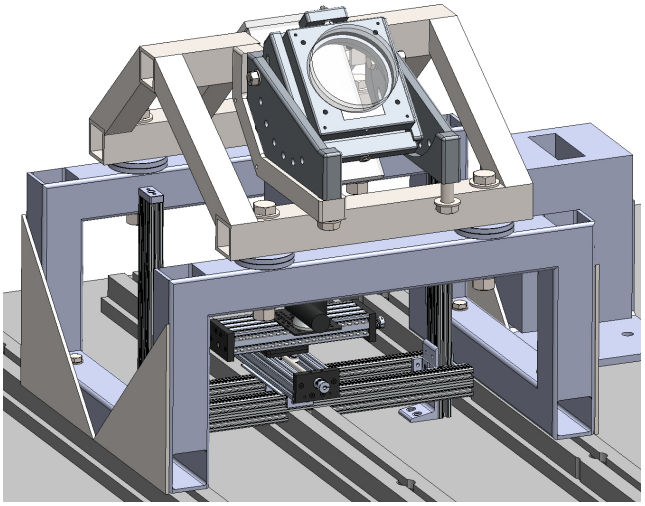

Figure 31. CAD angle view of target frame.

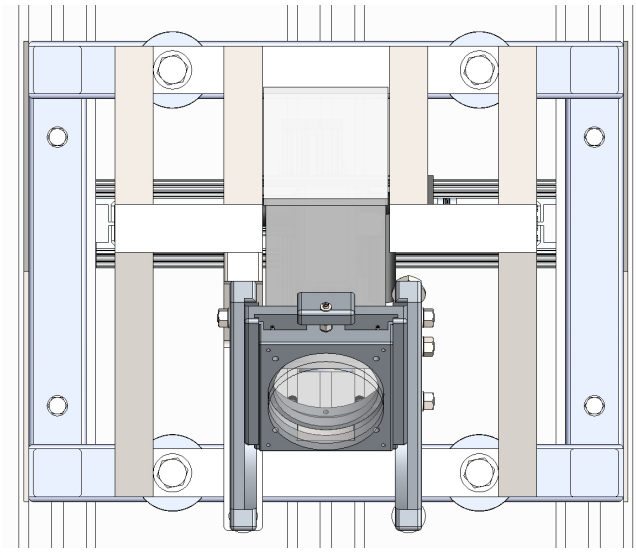

Figure 32. CAD top view of target frame.

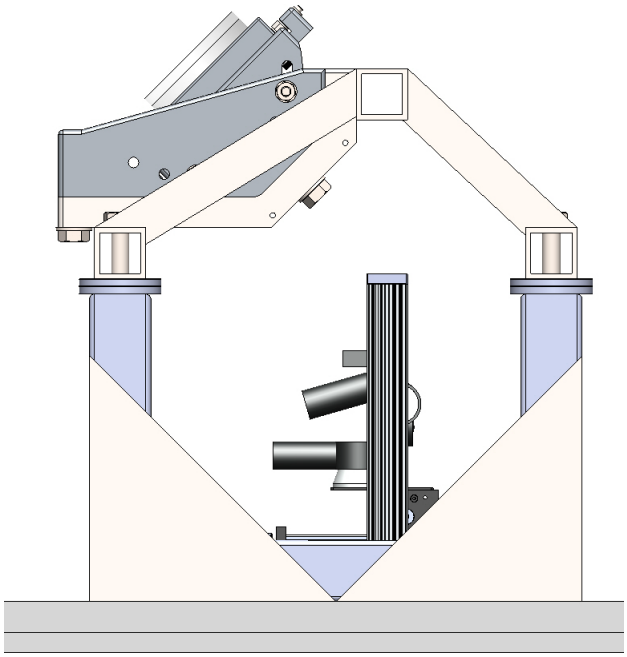

Figure 33. CAD side view of target frame.

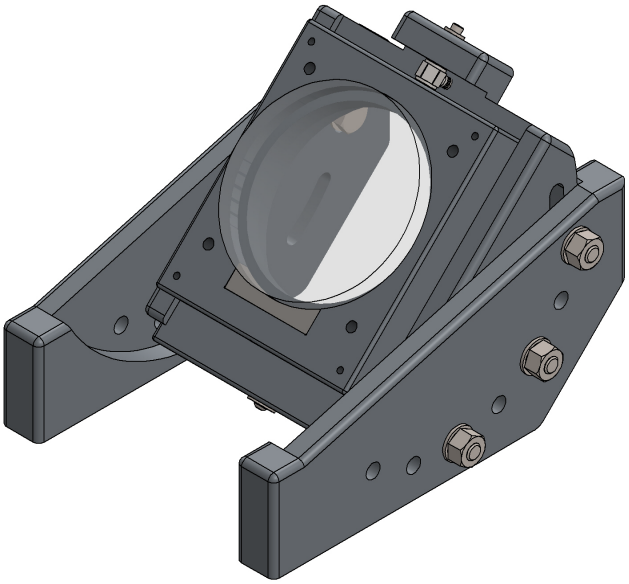

Figure 34. CAD view of variable angle target mount.

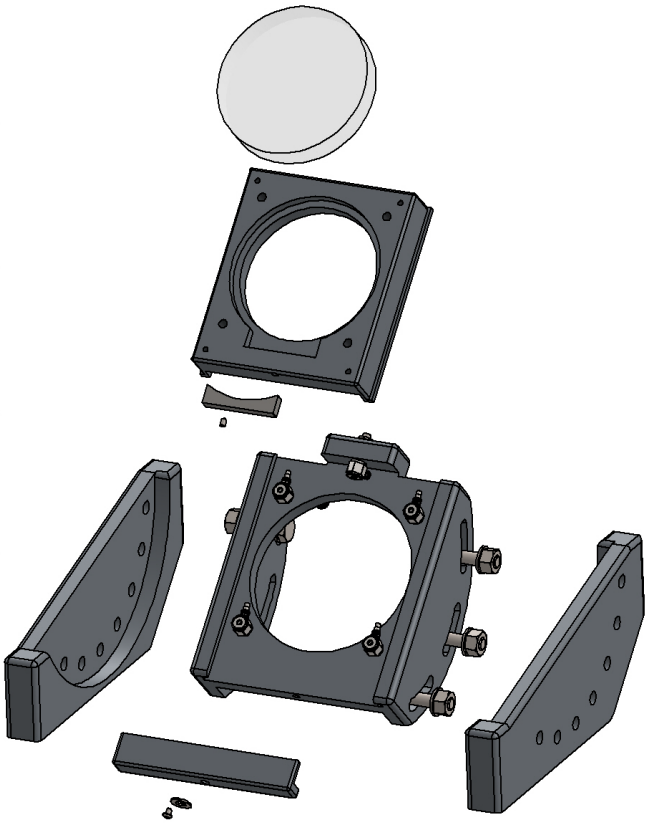

Figure 35. CAD exploded view of variable angle target mount.

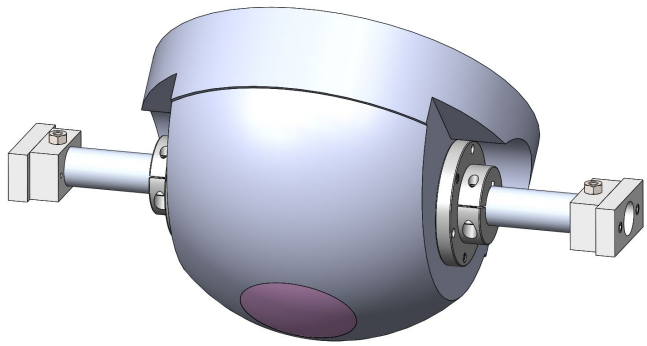

Figure 36. CAD view of vehicle assembly.

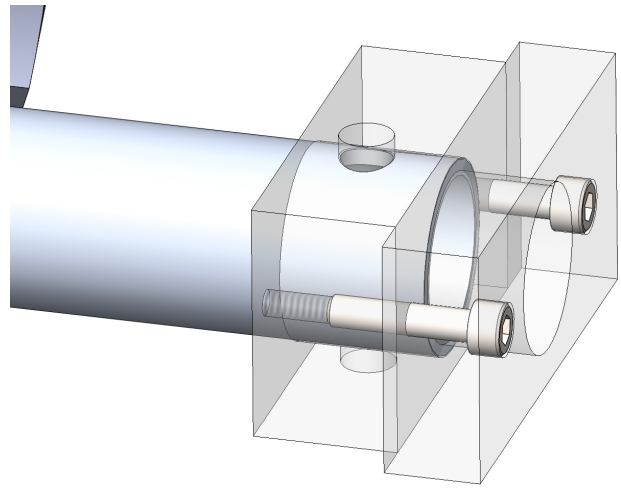

Figure 37. CAD detail of the mating blocks on the end of the vehicle assembly.

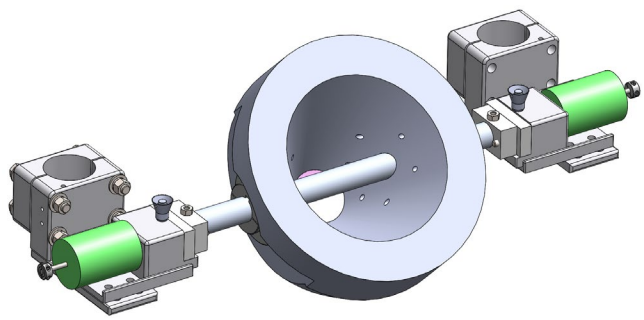

Figure 38. CAD view of vehicle assembly as it mates to the ends of the pendulum arms.

Appendix C: Images of the Pendulum Apparatus

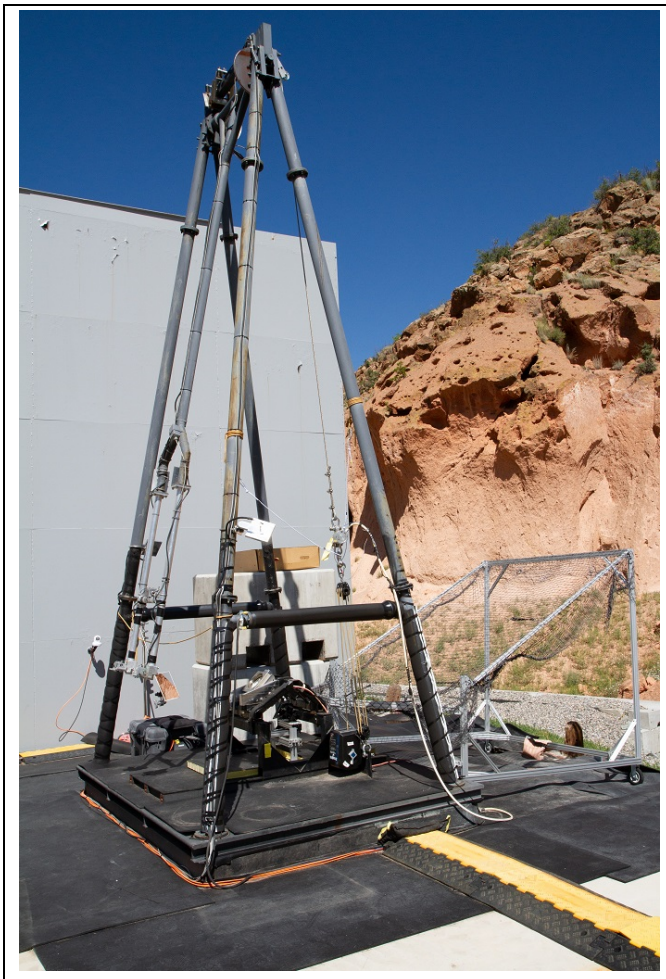

Figure 39. Pendulum photo.

Figure 40. Photo of pendulum. High-speed detail view video camera is visible to left.

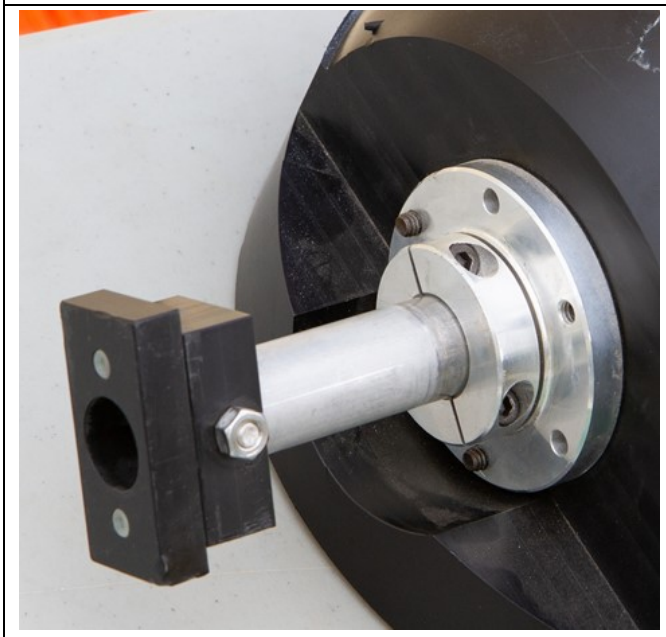

Figure 41. Detail view of vehicle mounting blocks.

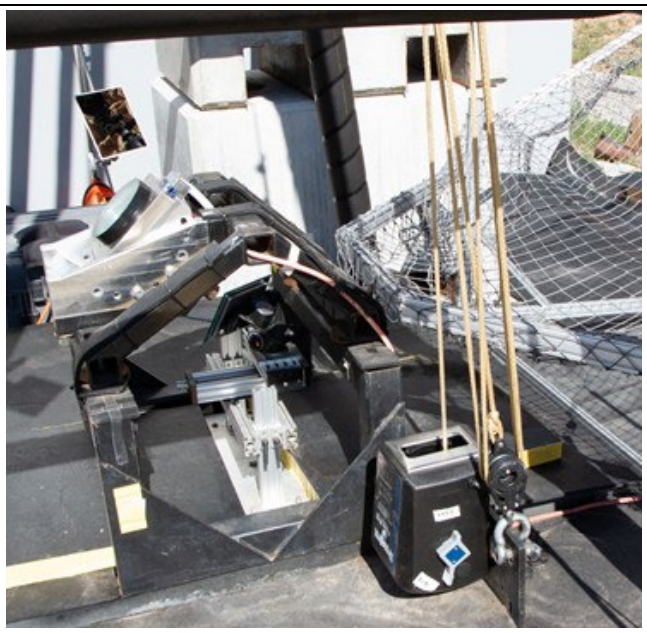

Figure 42. Winch setup for hoisting.

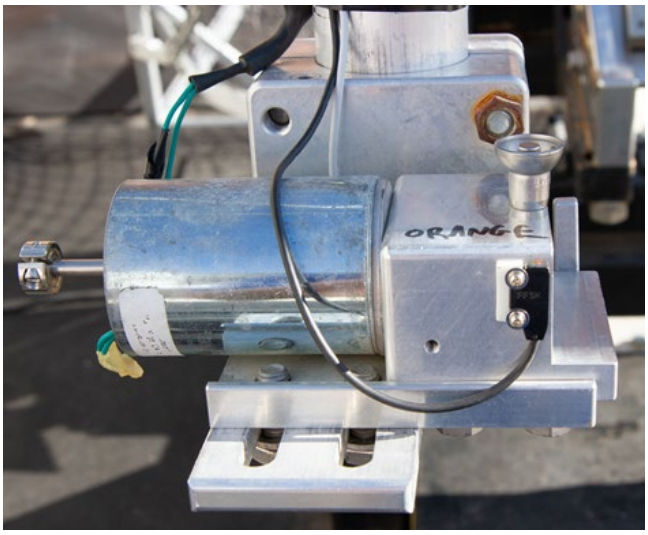

Figure 43. View of the solenoid release. The vehicle mounting blocks rest on the ledge on the right side.

Figure 44. View of the mirror setup below the target.

Figure 45. View of the pneumatically operated arm release latch.

Figure 46. Close-up view of the latch.

Figure 47. View of the top of the pendulum, showing the braking mechanism to the left, and the hoisting disc on the right.

Appendix D: Rex Gauge Company Durometer

12/19/2019 Model 2000 Max-Hand Durometer - Rex Gauge Durometers

Model 2000 Max-Hand Durometer

$545.00 – $800.00

Available Types:

A, D, B, C, DO, E, O

Features:

Includes NIST Calibration Certificate
Conforms to ASTM D-2240
Custom Made Carrying Case
Jeweled Movement
Holds Reading Until Reset

Type A	$545.00
Type D	$545.00
Type B	$595.00
Type C	$595.00
Type DO	$595.00
Type E	$800.00
Type O	$595.00

Description

The Max-Hand 2000 durometer is Rex Gauge Co.'s latest innovation for the testing of specimens with creep. The Max-Hand 2000 has a max- hand and an active hand for observing the creep characteristics of a specimen. What makes the Model 2000 unique is the magnetic-drag maximum reset mechanism. The user simply rotates the reset knob on the front of the gauge to clear the previous reading. The simplicity of the reset mechanism ensures a lifetime of use, and makes the Max- Hand 2000 the most affordable durometer for testing specimens with creep.

For Technical Information click here (/technical-information) or visit the ASTM at www.astm.org (http://www.astm.org).

Size: 2.25" x 6.125"H
Weight: 6 oz.

Features:

- Includes NIST Calibration Certificate
- Conforms to ASTM D-2240
- One Year Warranty
- Custom Made Carrying Case
- Holds Reading Until Reset
- Reads Maximum and Creep
- Cost Effective, Hand Operated
- Jeweled Movement